8-9-2006

# Microcracking Fracture Toughness for Graphite Epoxy Composite Laminates Using Finite Fracture Mechanics

Krishna Kumar Kasturi
*University of New Orleans*

# MICROCRACKING FRACTURE TOUGHNESS FOR GRAPHITE EPOXY COMPOSITE LAMINATES USING FINITE FRACTURE MECHANICS

A Thesis

Submitted to the Graduate Faculty of the
University of New Orleans
in partial fulfillment of the
requirements for the degree of

Master of Science
in
Mechanical Engineering

By

Krishna Kumar Kasturi

B. E, Osmania University, 2001

August 2006

# Acknowledgements

No Herculean task is consummated without the support and contribution from a number of individuals and that is the very essence of any colossal scheme. These few paragraphs are an effort to optimize my gratitude towards all those who helped me complete my thesis successfully.

If it were not my helpful professors I would never have had this unique opportunity and experience. I am so thankful to all my professors for their guidance throughout the course of my study at the University of New Orleans.

I was fortunate to get every sort of assistance and encouragement from my advisor **Dr. Paul J. Schilling**, who helped me congeal an ideal in its incipient, inchoate, amorphous form into a successful model. He is one of the most amicable persons I have ever come across. I would like to express my deepest appreciation towards him.

I am eminently grateful **Dr. Paul D. Herrington** and **Dr. Melody Verges** for being on my thesis committee. It was a great honor having them both.

I would like to thank my friends for being so supportive and understanding. My immense appreciation is to my wife Chaitanya Gampa who gave me invaluable support and encouragement whenever I felt lost. An unlimited gratitude is to my parents, sisters and brother who believed in me as I slogged along and motivated me to bring forth the peerless from me.

Without the prompt and able guidance from all these individuals, I could not have overcome the turbulence of time. Much is owed to them, much beyond words can express.

# Dedication

This work is dedicated to my parents and my wife, for their guidance, support, love and enthusiasm. Without these things this thesis could not have been possible.

# Table of contents

# List of Figures

# List of Tables

# Abstract

Graphite/epoxy composite laminates are widely used in the aerospace industry. However the industry cannot take full advantage of the superior strength and stiffness of composite materials until their failure mechanisms can be thoroughly understood by engineers. Recognizing the importance of such understanding, the current study was undertaken to determine the microcracking fracture toughness in composite laminates using the energy release rate criteria. Three materials of specific interest in the aerospace industry – IM7/977-2, IM7/5555 and IM7/5276-1 – were analyzed. To evaluate the microcracking fracture toughness, displacement controlled static tensile tests were performed. Microcrack density (the number of microcracks per unit length) was measured as a function of applied stress. The data were analyzed to obtain the microcracking fracture toughness ($G_m$) for each material system. The value of $G_m$ can be used to predict the microcracking behavior of composite laminates made from the corresponding material.

# 1. Introduction

## *1.1 Background and Motivation*

In recent years fiber-reinforced composite materials have been widely used in industry. Their advantages include high strength, high stiffness, unique flexibility in design capabilities and ease of fabrication. Besides, they are light weight, corrosion resistant, impact resistant, and have excellent fatigue strength. Today, fiber composites are used in such diverse applications as aircraft, space vehicles, automobiles, off-shore structures, containers and piping, electronics, sporting goods and appliances.

The word composite refers to the combination of two or more materials to obtain a unique combination of properties in the resulting material. These have high strength and stiffness to weight ratio and hence are used widely in aerospace and other critical applications. Composites exclude metal alloys, plastic co-polymers, minerals and wood.

The National Aerospace and Space Association (NASA) is developing a completely Reusable Launch Vehicle (RLV) in its mission of exploring outer space. This vehicle would make use of composites extensively. Liquid hydrogen (LH2*)* tanks are the largest structural components of RLV's. The design of lightweight fuel tanks is therefore important for reducing the cost of space access. Polymer Matrix Composite (PMC) hydrogen tanks have been proposed by Dixon [Ref 1] to reduce the weight of reusable launch vehicles. The fuel tanks of these vehicles would be manufactured mainly out of carbon/epoxy to reduce the weight. A study estimated that replacing a conventional fuel tank structure with an all composite one would reduce its weight by 40% and

the overall weight of the vehicle by 14% [Ref 2]. The purpose of these tanks is to hold liquid hydrogen at cryogenic temperatures around -423°F. Hydrogen is difficult to store because of its small molecular size and this makes it more prone to leakage. Many factors contribute to the leakage of the gases through the tank, like porosity, manufacturing flaws, and internal damage. Mostly in PMC materials leakage is believed to be because of microcracks which form leakage paths that allow the gases and liquid to pass through the material. It was also noted that the microcracks mostly occur in polymer matrix materials at -473°F (LH2*)* temperature because of large thermal residual stresses, large mechanical stresses and low transverse matrix strength [Ref 3]. Generally when the reusable launch vehicle is re-entering the atmosphere at high speeds of around mach 15 with empty fuel tanks, these fuel tanks quickly reach around 260°F and this large variation in temperatures may result in crack initiation through the tanks. Since composites are composed of different ply layers oriented in different directions, a change in temperature will cause the layers to expand in different directions depending on the thermal expansion coefficients of both the fibers and the matrix material. This develops a high amount of strain energy that can be relieved with the formation of cracks. If any kind of inter-connectivity exists between the cracks in adjacent layers they tend to form a path for the fuel to leak and make the composite structure permeable.

## *1.2 Project Objectives*

Composites are generally used because their desirable properties could not be achieved by either of the constituent materials alone. These have high strength and stiffness to weight ratio and hence are used widely in aerospace and other critical applications. Industry cannot, however,

take full advantage of the superior strength and stiffness of composite materials until the failure mechanisms of composite materials can be thoroughly understood by engineers.

The object of the present thesis is to determine the micro-cracking fracture toughness for carbon fiber epoxy resin matrix advanced composite materials IM7/977-2, IM7/5555 and IM/5276-1. These materials were supplied by Lockheed Martin Corporation to investigate the microcracking behavior. Preliminary studies for these systems included loading each sample to some predetermined load and then inspecting it via X-ray microtomography [Ref 2]. The microcracking density obtained from this inspection then allowed for one point from each sample to be plotted on a microcracking density versus applied stress plot.

The primary aim of the study is to predict the microcracking fracture toughness for the material system. The procedure to obtain this data contains 3 steps:1) preparation of the samples, 2) tensile loading of the samples to failure, 3) stopping the tensile test at incremental steps to record the crack progression by scanning the external surface of the laminate with a optical microscope. The data analysis involves the use of energy release rate criteria to determine the microcracking fracture toughness.

## *1.3 Thesis Outline*

This thesis is divided into 5 chapters. Chapter 1 (the current chapter) includes an introduction to composites and their application, the motivation and background, project objectives and thesis outline. A literature is presented in Chapter 2. This includes experimental observations and theory related to microcracking initiation and propagation. The main topic is the use of finite

fracture mechanics in predicting matrix microcracking. Of particular interest is the definition of microcracking fracture toughness, Gm, and methods to determine its value. Chapter 3 includes the step by step explanation of the experimental procedure followed. Results, data analysis and discussion appear in Chapter 4. Finally the conclusions drawn from the experimental results and recommendations in carrying out further research are presented in Chapter 5.

# 2. Literature Review

The purpose of this literature review is to provide background information on the issues to be considered in this thesis and to emphasize the relevance of this present study. The topics covered in this chapter are 1) composites and their constituents, 2) damage incurred in composites during the manufacturing processes or during service, 3) matrix microcracking, 4) finite fracture mechanics and the mathematical formulation for the determination of microcracking fracture toughness (Gm).

## *2.1 Composites and their constituents*

There are four categories of structural materials: metals, polymers, ceramics, and composites. Composites are made of various combinations of the other three materials in a macroscopic structural unit form. They mainly consist of a matrix material and a reinforcing material. Composites are generally used because their desirable properties could not be achieved by either of the constituent materials alone. A common example of this is the fibrous composite consisting of reinforcing fibers embedded in a binder, or matrix material. Fibrous reinforcement is more effective than others because many materials are much stronger and stiffer in fiber form than they are in bulk form. Fibers alone, however, cannot support longitudinal compressive loads and transverse loads. Thus, they must be held together with a binder or matrix to form a basic structural unit which we call a laminate. Then, a laminate is formed to carry general loads with individual continuous fiber/matrix lamina oriented toward pre-determined directions and bonded together. Generally in composites the reinforcements carry 70 to 90% of the load, and provide stiffness, strength, thermal resistance and other properties. The matrix material transfers the load

to the reinforcements, provides protection to the reinforcements against chemical and mechanical damage and gives the final desired shape to the composite. Generally reinforcement fibers are subjected to damage during handling and processing due to rupture against each other and the equipment. Hence the fibers are covered with a protective substance called as sizing. Sizing acts as a lubricant and helps a bundle of fibers to stick together and also helps in bonding with the matrix material. Generally sizing is preferred for glass fibers rather than carbon fibers.

### *2.1.1 Fiber Materials*

Glass fibers: By blending quarry products (sand, kaolin, limestone, and colemanite) at 1600°C, liquid glass is formed. The liquid is passed through micro-fine bushings and simultaneously cooled to produce glass fiber filaments from 5-24μm in diameter. The filaments are drawn together into a strand (closely associated) or roving (loosely associated), and coated with a "size" to provide filament cohesion and protect the glass from abrasion.

By variation of the recipe, different types of glass can be produced. The types used for structural reinforcements are as follows:

a. E-glass (electrical) – E-glass has lower alkali content and stronger than A-glass (alkali). It exhibits good tensile and compressive strength and stiffness, good electrical properties and relatively low cost, but impact resistance relatively poor. E-glass is the most common form of reinforcing fiber used in polymer matrix composites.
b. C-glass (chemical) – C-glass has the best resistance to chemical attack. It is mainly used in the outer layer of laminates used in chemical and water pipes and tanks.

c. R, S or T-glass – These are manufacturer's trade names for equivalent fibers having higher tensile strength and modulus than E-glass, with better wet strength retention. Higher ILSS (Interlaminar shear strength) and wet out properties are achieved through smaller filament diameter.

Carbon/Graphite fibers: Carbon fiber is produced by the controlled oxidation, carbonization and graphitization of carbon-rich organic precursors, which are already in fiber form. The most common precursor is polyacrylonitrile (PAN), because it gives the best carbon fiber properties, but fibers can also be made from pitch or cellulose. Variation of the graphitization process produces either high strength fibers (at ~2600°C) or high modulus fibers (at ~3000°C) with other types in between. Once formed, the carbon fiber has a surface treatment applied to improve matrix bonding and chemical sizing which serves to protect it during handling.

Carbon fibers are usually grouped according to the modulus band in which their properties fall. These bands are commonly referred to as: high strength (HS), intermediate modulus (IM), high modulus (HM) and ultra high modulus (UHM). The filament diameter of most types is about 5-7 μm. Carbon fiber has the highest specific stiffness of any commercially available fiber, very high strength in both tension and compression and a high resistance to corrosion, creep and fatigue. Their impact strength, however, is lower than either glass or aramid, with particularly brittle characteristics being exhibited by HM and UHM fibers.

Aramid fibers: Aramid fiber is a man-made organic polymer (an aromatic polyamide) produced by spinning a solid fiber from a liquid chemical blend. The bright golden yellow filaments produced can have a range of properties, but all have high strength and low density giving very high specific strength. All grades have good resistance to impact, and lower modulus grades are

used extensively in ballistic applications. Compressive strength, however, is only similar to that of E-glass.

Although most commonly known under its Dupont trade name ‘Kevlar’, there are now a number of suppliers of the fiber, most notably Akzo Nobel with ‘Twaron’. Along with the high strength properties, the fibers also offer good resistance to abrasion, and chemical and thermal degradation. However, the fiber can degrade slowly when exposed to ultraviolet light.

Other fibers: There are a variety of other fibers, which can be used, in advanced composite structures but their use is not widespread. These include: Polyester, Polyethylene, Quartz, Boron, and Ceramics.

### *2.1.2 Matrix Materials*

For the matrix, many modern composites use thermosetting or thermoplastic resins. The use of plastics in the matrix explains the name 'reinforced plastics' commonly given to composites. The plastics are polymers that hold the reinforcement together and help to determine the physical properties of the end product.

Thermoset matrices: Thermosets are formed by an irreversible chemical reaction called curing, in which they form 3D molecular cross-links in the form of chains which prohibit them from reforming and remolding once cured. These thermosets shrink once they are cured and hence induce internal stresses, cracking, fiber misalignment and dimensional inaccuracy to the composite. These are easy to process as they have low viscosity.

Thermoplastic matrices: Thermoplastics are softened from solid state to be processed and they have high viscosity and need high temperatures for softening which makes them difficult to process. These do not undergo any curing process and hence these can be repaired by reforming and remolding.

Other matrices: Ceramics, carbon and metals are used as the matrix for some highly specialized purposes. For example, ceramics are used when the material is going to be exposed to high temperatures (eg: heat exchangers) and carbon is used for products that are exposed to friction and wear (eg: bearings and gears).

The main concern of this thesis is on carbon–epoxy composites and their damage during tensile testing. Here carbon fibers act as the reinforcing material and epoxy as the matrix material. Carbon fibers have excellent chemical resistance and high strength along the axial direction. Carbon–epoxy composites can be manufactured using any of the available processes in the market like hand lay-up, vacuum bagging, autoclave processing, compression molding, resin transfer molding (RTM), and pultrusion.

The samples which are used in this research were cut from panels of carbon-epoxy composite manufactured by hand lay-up and vacuum bagging at the Lockheed Martin Corporation. Different types of damage occur in composites which might be due to the manufacturing process or due to the load application in service.

## *2.2 Damage in Composites*

Damage to composites is often hidden to the eye. Where a metal structure will show a dent or ding after being damaged, a composite structure may show no visible signs of damage, and yet may have delaminated plies or other damage within. It is well known that the defects and damage in laminated composites reduce the strength, stiffness and also the safe working life of the composite structures. Defects may be introduced during manufacture, accidentally in-service or perhaps unavoidably in design because of the requirement to introduce discontinuities such as cutouts, ply drops or structural connections [Ref 6, 7].

The defects commonly introduced to composite materials during manufacturing and processing are inclusions, de-bonding, fiber misalignment, voids and residual stresses.

a. *Inclusions* – Accidentally included materials during manufacturing like peel paper can have a degrading effect on the mechanical properties.
b. *De-bonds* –The failure of the interface between the fibers and the matrix material which leads to separation between them, called de-bonding. de-bonding can occur because of poor consolidation or as a result of an inclusion.
c. *Fiber misalignment* – This is damage especially prevalent in low fiber volume fraction materials.
d. *Voids* – Voids are due to inclusion of air, solvents or other contamination during mixing of resin.
e. *Residual stresses* – These stresses are mainly caused by the curing process. These affect the mechanical properties and can cause warping, fiber buckling, microcracking of the matrix and delamination. The cause of these stresses is mainly

the difference in thermal expansion of the fiber and matrix material in different directions.

The most common defects introduced in composite materials during service loading are matrix cracking, fiber breakage, fiber pull-out, delamination, and fiber-matrix de-bonding. *Figure 2.1* shows a composite panel, with 0º plies on the outside and the 90 º plies in the inside, uniaxially loaded to a stress of $\sigma_x$. The types of damage incurred in the composite laminate due to this uniaxial tensile loading are discussed below.

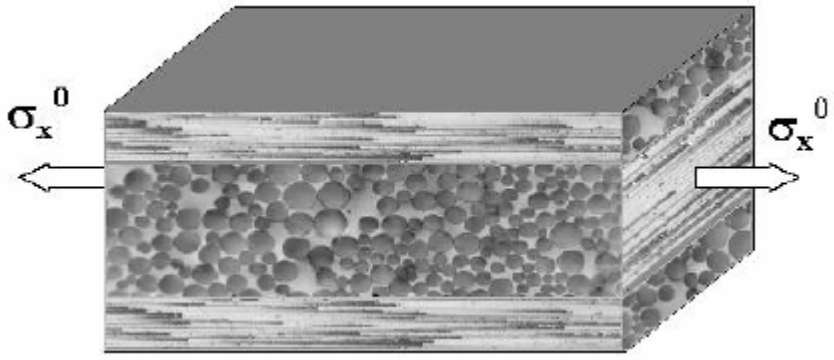


***Figure 2.1*** *Cross-ply laminate subjected to uniaxial loading [Ref 8]*

*Fiber-matrix debonding*: This is the first mode of failure that occurs in the composite material when uniaxially loaded because of the poor interface bonding between the fibers and the matrix. These debondings link together to form large scale damage called matrix cracking. *Figure 2.2* shows a matrix crack formed due to fiber-matrix debonding.

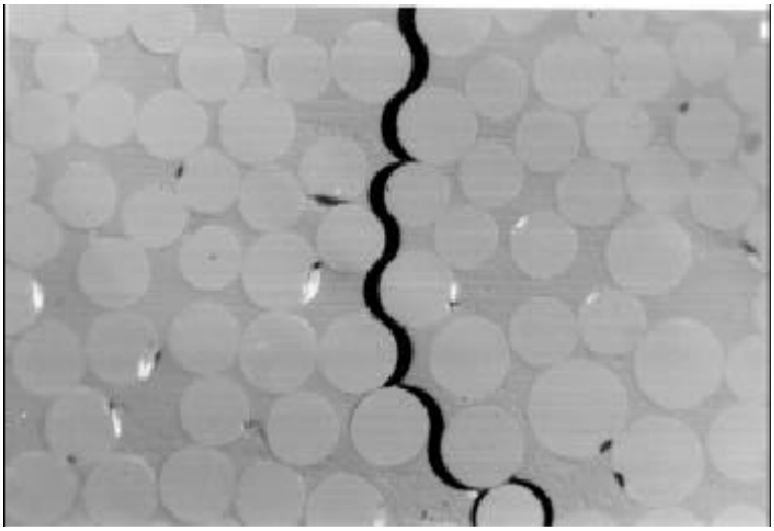

***Figure 2.2*** *Propagation of a matrix cracking due to fiber-matrix debonding [Ref 8]*

*Matrix cracking*: As described by R.Joffe [Ref 8], the cracks are initiated from the interface failures. Transverse cracks or matrix cracks are formed as a result of multiple debonding between the fibers and matrix. These microcracks are catastrophic because they reduce the load carrying capacity of the structure in the direction normal to the cracks and reduce the stiffness in that direction. *Figure 2.3* shows matrix cracking of a cross-ply laminate subjected to uniaxial tension.

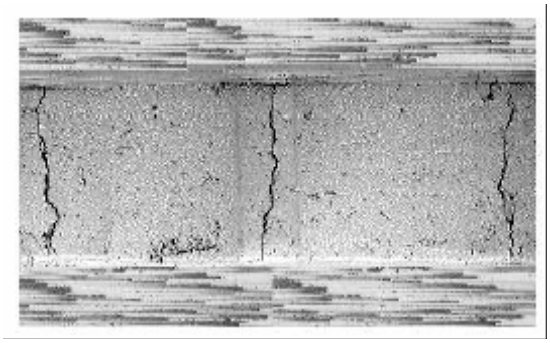

***Figure 2.3*** *Matrix cracking in a cross-ply laminate [Ref 8]*

*Delamination*: Delamination is a form of failure that occurs on a plane between adjacent layers within a laminate. Microcracks introduce multiple stress concentration points at the crack tips as the microcracks are restrained by the adjacent layers. These crack tips exist at the interface between plies of a laminated composite and thus lead to delamination which is large scale damage. Delamination can increase connectivity of the matrix cracks and cause leakage paths to fuel when the structure is used as a pressure vessel.

*Fiber breaking*: Microcracks in composites are formed because of the poor interfacial bonding when subjected to tensile loading. These microcracks lead to delamination, and fiber breaking would be the next mode of failure after delamination. Since the adjacent layers with no microcracks tend to bear the entire applied load, their fibers tend to crack leading to fiber breakage.

*Fiber pull-out*: This damage occurs prior to fiber breakage. The fibers get pulled out of the matrix on tensile loading.

*Fracture*: This is the final stage of failure and the material breaks and separates out. Fracture might be in the form of complete detachment of the materials or constrained ply cracking.

*Figure 2.4* shows the various types of damage observed in a composite material when subjected to uniaxial loading. The modes of damage shown in *Figure 2.4* are based on the information collected from various researchers and their publications.

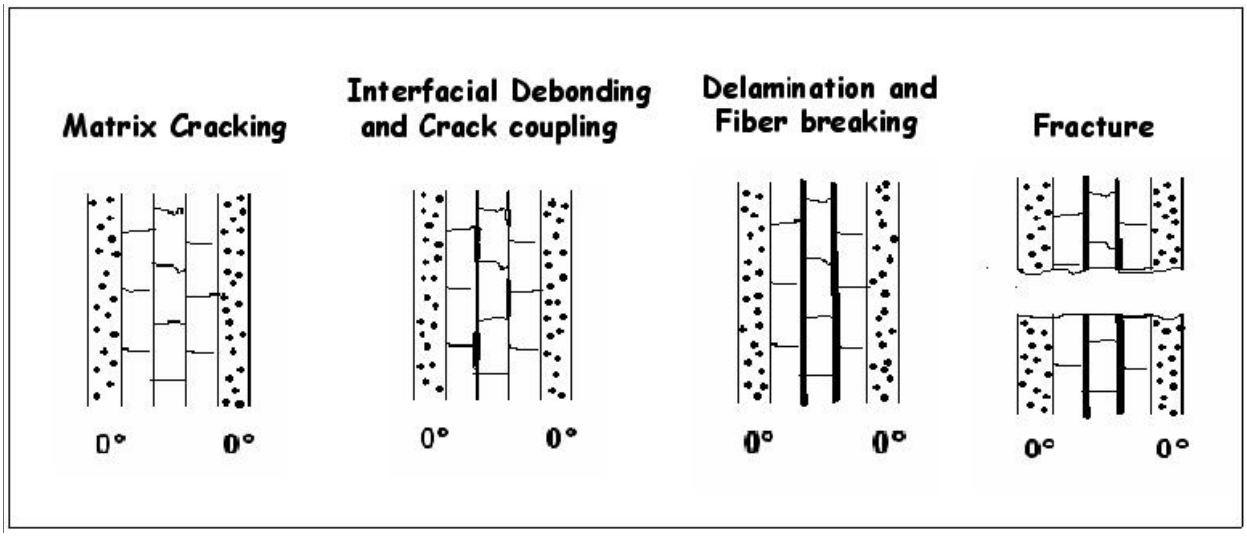


***Figure 2.4*** *Modes of damage in a composite material [Ref 9]*

## *2.3 Microcracking*

As described earlier, the first form of damage in composite laminates is usually microcracking or transverse cracking [Ref 10]. Microcracks not only change the thermal and mechanical properties of laminates, but also present pathways through which corrosive agents may penetrate into the interior of the laminate. Perhaps most importantly, microcracks act as nuclei for further damage such as delamination, longitudinal splitting [Ref 11, 12], and curved cracks [Ref 13]. Microcracking is the cracking of the matrix material due to transverse loading in the cross-ply laminates. These microcracks run all the way through the thickness of the ply and parallel to the fibers in the ply and are usually transverse to the main loading direction and thus also called transverse cracks. The term matrix microcracks, microcracks, intra-laminar cracks, ply cracks, and transverse cracks are used interchangeably in the composite literature.

Microcracks can develop during tensile loading, during fatigue loading, during changes in temperature and during thermo-cycling. Microcracks due to thermal loading or thermal residual

stresses are formed due of the difference in the thermal expansion coefficient between the fibers and the matrix material. Generally the matrix material has a greater thermal expansion coefficient than the fibers. When a thermal load is applied to the composite, due to this difference in thermal expansion coefficient, the matrix material tries to expand more than the fibers and this leads to de-bonding of matrix with the fibers at the weakest matrix-fiber interface region. Further application of this thermal load leads to large scale damage, called matrix microcracking.

As mentioned earlier microcracking degrades the thermo-mechanical properties of the laminate and hence often leads to overall failure. The first microcrack causes very little degradation in the thermo-mechanical properties of the composite laminate but upon continued loading the laminate tends to crack more forming multiple microcracks. This multiple microcracking causes more degradation in the thermo-mechanical properties of the laminate. The growth of multiple microcrackings was explained by Groves et al [Ref 13]. At low crack density, both the maximum axial stress and the maximum principle stress in the 90º plies occur midway between the existing microcracks. Thus at low crack density the new cracks try to form midway between the existing cracks and develop into periodic array of cracks as shown in *Figure 2.5*.

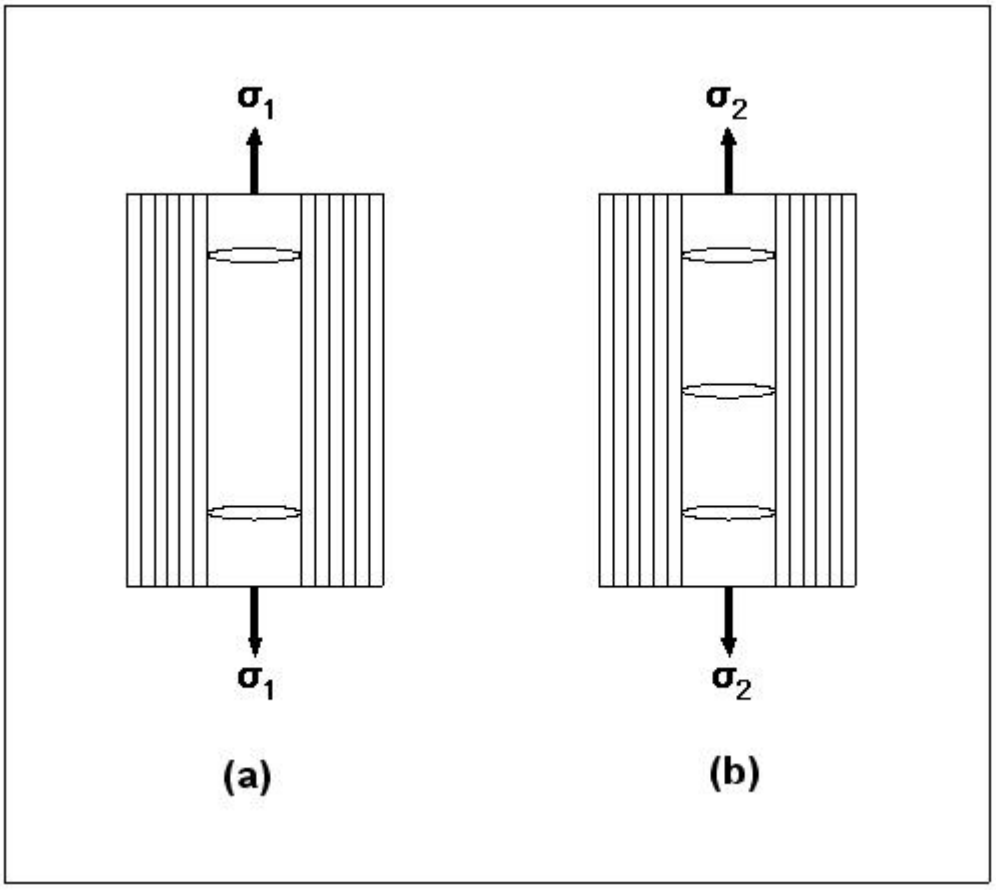


***Figure 2.5*** *Schematic of microcrack development in the 90° ply at different stress levels. (a) Microcrack development at an applied load* $\sigma_1$. *(b) Formation of microcrack in the middle of existing cracks at applied load* $\sigma_2$ ($\sigma_2 > \sigma_1$).

Garrett and Bailey [Ref 14-16] have performed many experiments on glass reinforced polyester $[0/90]_s$ and glass reinforced epoxy $[0/90]_s$ laminates to calculate the strain required to initiate microcracking in composite materials. They continuously varied the thickness of the 90º plies keeping the thickness of the supporting 0º plies constant and their results indicate that on decreasing the thickness of the 90º plies less than that of the 0º plies, the strain to initiate microcracking in the 90º plies increases. At a certain decrease in thickness of the 90º plies the

cracks were partially and totally suppressed. Similar experiments were conducted on the carbon-epoxy laminates by Bailey, Curtis and Parvizi [Ref 11, 12] and found that the strain to initiate microcracking increases as the thickness of the 90º plies decreases.

Experiments were also conducted on $[90n/0m]_s$ laminates [Ref 17-23] (with the 90° plies on the outside). These results show that the strain to initiate microcracking in the $[90n/0m]_s$ is lower than in the $[0m/90n]_s$ laminates with the 90° plies in the middle. This result can be supported as the surface 90º plies in the [90n/0m]s laminates are constrained only on one side by the adjacent 0º plies where as in the [0m/90n]s laminates the 90º plies are constrained on both sides. *Figure 2.6* shows the schematic of the microcrack behavior in the $[0n/90m]_s$ and $[90m/0n]_s$ laminates.

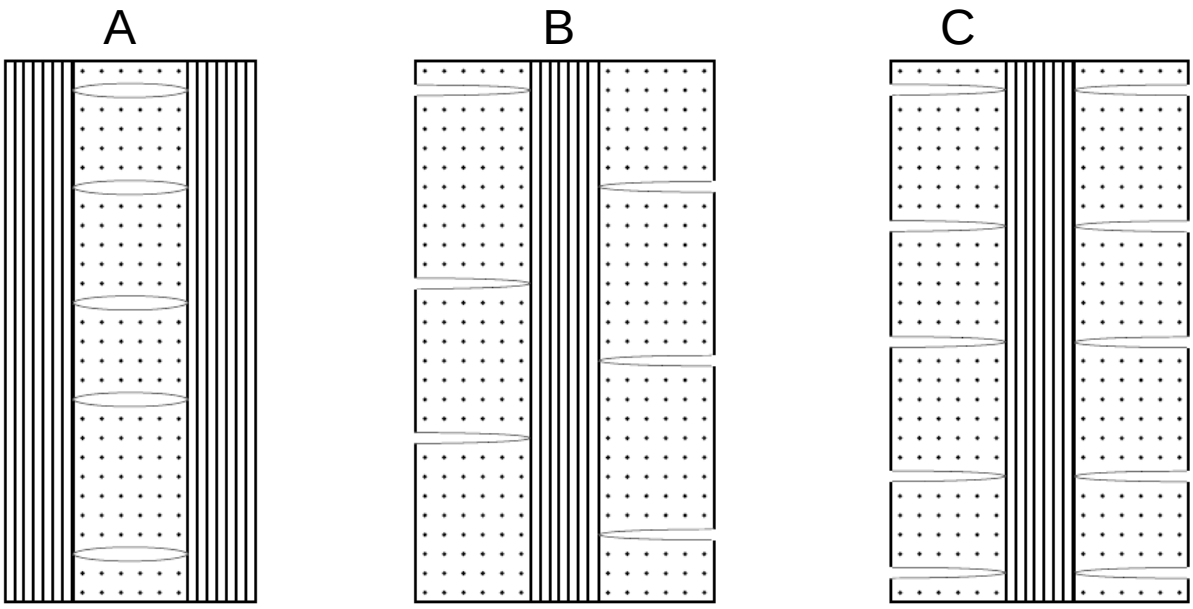


***Figure 2.6*** *The characteristic damage state of A: [0n/90m]s laminate, B: [90m/0n]s laminate having "staggered" or anti-symmetric microcracks, C: [90m/0n]s laminate having symmetric microcracks (this symmetric damage state is sometimes assumed in analyses but is never observed in experiments.)*

Many carbon-epoxy laminates with different ply orientations were also tested by Flaggs and Kural [Ref 24]. In the experiments conducted [Ref 11, 12, 24], the microcracks in the carbon-epoxy laminates always formed instantaneously across the entire cross sectional area of the 90º plies. The thinnest of the 90º plies tested was half the thickness of the 0º plies and they could see no partial or total suppression of the microcracks [Ref 24].

## *2.4 Finite Fracture Mechanics*

As discussed in the previous sections, microcracks can lead to delamination, cause fiber breaks, and provide pathways for entry of corrosive liquids. An important issue in design of composite laminates is to be able to predict the initiation and development of microcracking damage following complex loading conditions. A complicating feature of composite fracture mechanics analysis is that laminates often fail by a series of fracture events instead of by continuous crack growth. When cross-ply laminates are loaded in tension, the microcracking process is a series of events in which a single microcrack forms and instantaneously (on an observation time scale) propagates until it fills the entire cross-sectional area of the ply. Conventional fracture mechanics deals with predicting the propagation of an existing crack. One could imagine analyzing microcrack propagation within a ply by standard methods, but there is little incentive to tackle this problem. The analysis could not be compared to experimental results for events and the analysis of a single crack does not answer the problem of predicting the extent or number of microcracks that form under various loading histories [Ref 25]. Some microcracking models have abandoned fracture mechanics and used critical stress criteria instead; these models do not work well [Ref 26]. A better approach is to extend fracture mechanics methods to handle fracture events. Hashin has coined the term “finite fracture mechanics” to describe prediction of fracture

events by comparing the total energy released due to a finite amount of crack area to event toughness [Ref 27]. A finite fracture mechanics model for matrix microcracking can correlate a large body of experimental observations and can predict the extent of microcracking damage under various loading conditions [Ref 28, 29].

### *2.4.1 Finite Fracture Mechanics Principles*

As described by Nairn [25], the development of a finite amount of fracture area, $\Delta A$, must conserve energy. By the first law of thermodynamics, energy balance for an elastic material can be expressed as below.

$$\frac{\Delta w}{\Delta A} - \frac{\Delta U}{\Delta A} = 2\gamma + \frac{\Delta K}{\Delta A}$$

Where $w$ is external work, $U$ is internal energy, $\gamma$ is surface energy, and $K$ is kinetic energy. Conventional fracture mechanics deals with infinitesimal static crack growth for which $\Delta A \to da$ and $\Delta K \to 0$. Crack growth occurs when energy release rate, $G$, is equal to the critical energy release rate, $G_c$.

$$G = \frac{dw}{dA} - \frac{dU}{dA} = 2\gamma = G_c$$

$G_c$ is used in place of $2\gamma$ because experimental observations show that energy released during crack growth is always much larger than the thermodynamic surface energy ($2\gamma$). In other words, $G_c$ *is* an *effective* material property that accounts for crack-tip energy dissipation not included in a linear-elastic stress analysis of crack-tip stresses. The logical extension to finite fracture mechanics is to assume a fracture event occurs when the finite energy release rate is equal to the critical material property or fracture toughness ($G_m$).

Conventional fracture mechanics works well provided $G_c$ is found to be independent of sample geometry. Similarly, finite fracture mechanics works well provided $G_m$ is independent of sample geometry and current damage state and provided initiation of the event is facilitated by conditions such as existing flaws or stress concentrations.

### *2.4.2 Application to Microcracking*

To verify the use of finite-fracture mechanics for microcracking, predictions can be compared to experiments. The procedure is to evaluate fracture toughness and then predict microcrack formation by assuming the next crack forms when energy released is equal to the fracture toughness. A unique feature of finite fracture mechanics is that energy release rate, *G,* is different for load-control *vs.* displacement-control experiments [Ref 29, 30]. Most static experiments use displacement control, but fatigue or thermal cycling experiments use load control. Both conditions must be analyzed.

*Figure 2.7* shows the process of forming a new microcrack at some location between two existing microcracks. The thermoelastic variational mechanics analysis described by Nairn [Ref 31] gives the energy released due to the formation of the new microcrack illustrated in *Figure 2.7b*.

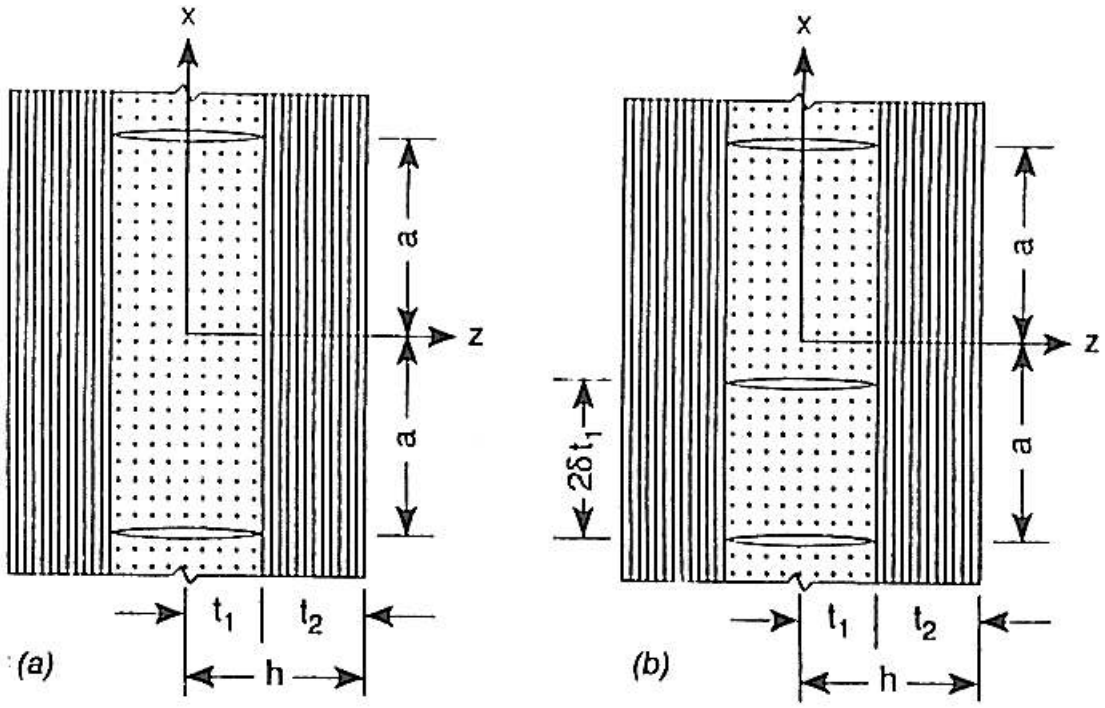


***Figure2.7*** *Edge view of a cross-ply laminate with microcracks. (a)Two microcracks in the $90^0$ plies (b) The formation of a new microcrack at a distance 2δt, above the bottom micro-crack [Ref 5]*

## *2.5 Mathematical Formulation of Fracture Mechanics*

According to Nairn and Liu [4] when a laminate is loaded by a tensile stress of $\sigma_o$ in the x-direction the nonzero stresses in the x-direction in both $0^o$ and $90^o$ plies are expressed as follows

$$\sigma_{x^0}^{(1)} = k_1 \sigma_0 \qquad (1)$$

$$\sigma_{x^0}^{(2)} = k_2 \sigma_0 \qquad (2)$$

Here $k_1$ and $k_2$ are effective stiffness and superscripts (1) and (2) denote stresses in $90^0$ and $0^0$ plies, respectively. These can be found by laminated plate theory or by constant strain assumption.

$$k_1 = \frac{E_T}{E_c} \qquad k_2 = \frac{E_A}{E_c} \tag{3}$$

$E_A$ and $E_T$ are the axial and transverse modulus of the ply material and $E_c$ is the x-direction modulus of the cross-ply laminate. Following Hashin [32, 33], Nairn made one assumption that the x-axis tensile stresses in each ply depend only on the axial coordinate x and are independent of the thickness coordinate z. Now the stresses in $90^0$ and $0^0$ plies will be

$$\sigma_x^{(1)} = \sigma_{(x^0)}^{(1)} - \psi_1(x) \tag{4}$$

$$\sigma_x^{(2)} = \sigma_{(x^0)}^{(2)} - \psi_2(x) \tag{5}$$

By submitting the above stress values into the equilibrium equations and using the obvious boundary conditions Nairn [Ref 5] derived ψ as below [Ref 31, 32 and33]

$$\psi = \left( \sigma_{x^0}^{(1)} - \frac{\Delta\alpha T}{C_1} \right)\phi + \frac{\Delta\alpha T}{C_1} \tag{6}$$

Where $\Delta\alpha = \alpha_T - \alpha A$, the difference between the transverse and longitudinal thermal expansion coefficients, T , stress free temperature, is the difference between the cure temperature and room temperature and φ is

$$\begin{aligned} \phi = & \frac{2(\beta \sin\alpha\rho\cos\beta\rho + \alpha\cosh h\alpha\rho\sin\beta\rho)}{\beta\sinh 2\alpha\rho + \alpha\sin 2\beta\rho}\cosh\alpha\xi\cos\beta\xi \\ & + \frac{2(\beta\cosh\alpha\rho\sin\beta\rho - \alpha\sinh\alpha\rho\cos\beta\rho)}{\beta\sinh 2\alpha\rho + \alpha\sin 2\beta\rho}\sinh\alpha\xi\sin\beta\xi \end{aligned} \tag{7}$$

In the above equation

$$\rho = a/t_1 \tag{8}$$

$$\xi = x/t_1 \tag{9}$$

$$\alpha = \frac{1}{2}\left(2q^{1/2} - p\right)^{1/2} \tag{10}$$

$$\beta = \frac{1}{2}\left(2q^{1/2} + p\right)^{1/2} \tag{11}$$

Where p and q are functions of $C_1$ –$C_4$, which are functions of the mechanical properties and thickness of the plies as described below;

$$p = \frac{(C2 - C4)}{C3} \tag{12}$$

$$q = \frac{C1}{C3} \tag{13}$$

$$C_1 = \frac{1}{E_T} + \frac{1}{\lambda E_A} \tag{14}$$

$$C_2 = \frac{\nu_T}{E_T}\left(\lambda + \frac{2}{3}\right) - \frac{\lambda \nu_A}{3E_A} \tag{15}$$

$$C_3 = \frac{\lambda + 1}{60E_T}\left(3\lambda^2 + 12\lambda + 8\right) \tag{16}$$

$$C_4 = \frac{1}{3G_T} + \frac{\lambda}{3G_A} \tag{17}$$

Using above equations and [Ref 5] the energy release rate, $G_{m,}$ is given by

$$G_m = \left(\frac{E_T}{E_C}\sigma_o - \frac{\Delta\alpha T}{C_1}\right)^2 C_3 t_1 Y(D) \tag{18}$$

Where $\Delta\alpha = \alpha_T - \alpha A$

Where $E_T$ and $E_C$ are the axial modulus of the ply material and the *x*-direction modulus of the cross-ply laminate, $\sigma_o$ is the tensile stress in the *x*-direction, $t_1$ is the thickness of the 90$^o$ ply $\Delta\alpha$ is the difference between the transverse and longitudinal thermal expansion coefficient, *C1*, *C3* are constants which are function of other material properties like $G_A$, $G_T$, $\nu_A$ ,$\nu_T$ (axial and transverse

shear modulus and Poisson's ratio respectively) and they are expressed later in this section. *Y (D)* is called the Energy Release Rate scaling as shown in Equation (19).

$$Y(D) = LW \frac{d}{dA} \frac{\sum_{i=1}^{N} \chi(\rho_i}{\sum_{i=1}^{N} \rho_i} \tag{19}$$

Y (D) is function of a new function called χ(ρ) which is dependent on the crack spacing and given by Equation (20)

$$\chi(\rho) = 2\alpha\beta(\alpha^2 + \beta^2) \frac{\cosh 2\alpha\rho - \cos 2\beta\rho}{\beta \sinh 2\alpha\rho + \alpha \sin 2\beta\rho} \tag{20}$$

Where ρ is defined as $a/t_1$ and $2a$ is the distance between the existing cracks, L, W and A are length, width and cross-section area of the sample $\alpha$ and $\beta$ are constants dependent on the material properties as described above.

Now considering a sample of with N microcracks and crack spacing between each crack is characterized as $\rho 1, \rho 2, \rho 3, \rho 4, \ldots\ldots \rho_N$ <χ(ρ)> is given as

$$< \chi(\rho) >= \frac{1}{N} \sum_{i=1}^{N} \chi(\rho_i) \tag{21}$$

And crack density D = N/L. After the formation of the new crack at *k*th interval at ξ= 2δ-$\rho_k$ and <χ(ρ)> is given as in equation below .And ξ is defined as $x/t_1$

$$< \chi(\rho) >= \frac{1}{N+1} \left[ \left( \sum_{i=1}^{N} \chi(\rho_i) \right) - \chi(\rho_k) + \chi(\rho_k - \delta) + \chi(\delta) \right] \tag{22}$$

And the crack Density D= (N+1)/L. By substituting $\chi(\rho)$ in *Y(D)* and *Y(D)* in Equation (18) we can find $G_m$.

Previous studies indicate that cross-ply laminates tend to form regularly spaced microcracks; during a typical experiment, it is not know where the next new crack will form. Assuming the next new microcrack forms in the crack interval whose spacing is equal to the average crack spacing, $\rho_k$ , can be expressed as $\rho_k = 1/2t_1D$.And also assuming the new crack forms at the mid-span of the existing crack interval $\delta$ can be expressed as $\delta=\rho/2$. With these assumptions the function Y (D) becomes as below.

$$Y(D) = 2\chi(\rho/2) - \chi(\rho) = 2\chi\left(\frac{1}{4t_1D}\right) - \chi\left(\frac{1}{4t_1D}\right) \tag{23}$$

The above equation is consistent with the assumptions made earlier and with real experimental observation that when the crack density (D) is low, the energy release rate is constant. In this low crack density area the energy release by the formation of new crack formed between the two existing cracks is independent of crack spacing. But when the crack density gets higher and there is distribution of crack spacing, energy released by the formation of the new microcrack in a small crack interval will be lower than the energy released by the formation of new microcrack in a large crack interval. So Nairn and Liu introduced a new parameter $f$ and modified the Equation (23) to

$$Y(D) = 2\chi(f\rho/2) - \chi(f\rho) = 2\chi\left(\frac{f}{4t_1D}\right) - 2\chi\left(\frac{f}{4t_1D}\right) \tag{24}$$

Where $f>1$, is the average ratio of the size of the crack interval in which the crack forms to the average crack spacing. Also an equation has been developed to back calculate the stress applied with a constant value of Gm, Which is simply derived from Equation (18) and is shown in Equation (25)

$$\sigma_0 = \frac{E_C}{E_T}\left(\left[\frac{Gm}{C_3 t_1 Y(D)}\right]^{1/2} + \frac{\Delta\alpha T}{C_1}\right) \tag{25}$$

### *2.5.1 Effects of parameter f*

As mentioned, in certain situations we have to deviate from the assumption of the next microcrack will tend to form in a crack interval whose spacing is equal to the average crack spacing ( that the cracks tends to form in the middle of existing crack interval). Several methods have been reported in previous studies by Narin [Ref 34] in calculating or estimating the value of parameter *f*. One of which is an integral approach, in which he treated Equations (24) and (25) as single-parameter representations of Y (D) and developed the first order differential equation

$$\frac{d < \chi(\rho) >}{dD} = \frac{2\chi(f < \rho > / 2) - \chi(f < \rho >) - < \chi(\rho) >}{D} \tag{26}$$

This first order differential equation can easily be integrated to predict <χ(ρ)> as a function of D for any value of "*f*". By comparing the prediction to experimental results it is possible to measure "*f*" and a typical curve to compare the experimental results to the predicted results has shown in *Figure2.8*.

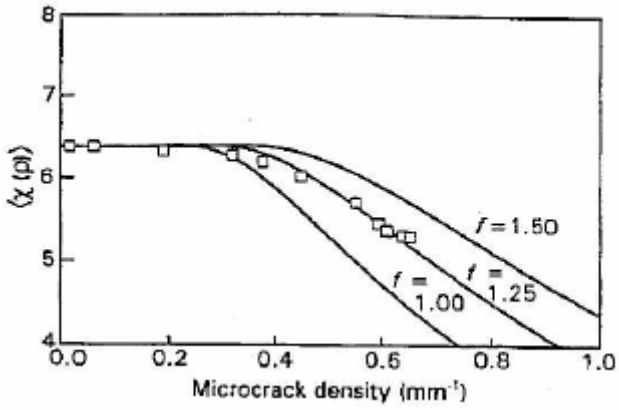


***Figure2.8*** *The energy release rate scaling function, χ (ρ), as a function of the crack density for f=1.00, f=1.25 and f=1.50 [Ref 34]*

From the *Figure 2.8* it is evident that when the crack density is low the energy release rate is constant. In this regime, the energy released by the formation of a new microcrack between any two existing microcracks will be independent of the crack spacing. As the crack density gets high and there is a distribution of crack spacings. The energy released by formation of a microcrack in a small crack interval will be lower than the energy released by the formation of a microcrack in a large crack interval. By the energy release rate criterion, this effect suggests that at high crack densities, the microcracks will prefer to form in larger crack intervals than the average crack interval. Thus equation (23) has been modified to equation (24) to account this effect.

## *2.6 Master Curve Analysis*

A master curve for microcracking experiments is typically represented by a plot of reduced stress ($\sigma_R$) against reduced crack density ($D_R$). The terms reduced stress and reduced crack density were derived [Ref 34] from the energy release rate (microcracking fracture toughness), $G_m$ , equation (18) from previous section and they can be expressed as follows.

$$\sigma_R = -\frac{k_m^{(1)}}{k_{th}^{(1)}}\sigma_0 \tag{27}$$

$$D_R = -\frac{1}{k_{th}^{(1)}}\left(\frac{1}{C_3 t_1 Y(D)}\right)^{1/2} \tag{28}$$

Where $k_m^{(1)} = \frac{E_T}{E_C}$ and $k_{th}^{(1)} = \frac{\Delta\alpha}{C_1}$

According to Nairn [Ref 34] if the variational analysis and energy-release-rate failure criterion are appropriate, a plot of $\sigma_R$ against $D_R$ will be linear with slope $(G_m)^{1/2}$ and intercept T. Because $G_m$ and T are lay-up independent material properties, the result from all laminates of a single material with the same processing conditions should fall on the same linear master curve. A critical test of the variational analysis microcracking theory is to determine if the master curve is linear and if all laminates fall on the same line.

A typical master-curve analysis for a single laminate is shown in *Figure2.10* [Ref 34] just to explain the significance of the slope and the intercept. The master plot is linear except for few points at the lowest crack density as the low crack density results are affected by processing flaws that are not specifically included in the microcracking analysis [Ref 5]. The straight line in the *Figure2.10* is the best linear fit that ignores the low crack density data and the slope of represents the value of $(G_m)^{1/2}$.

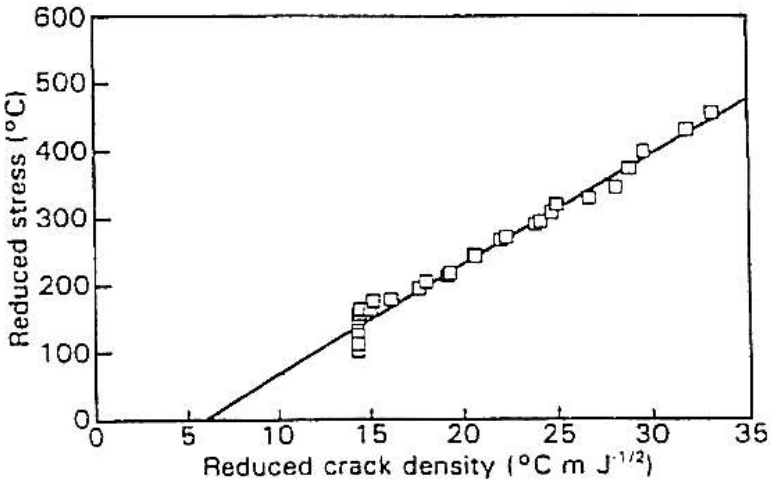


***Figure2.10*** *A master-curve analysis of a laminate [Ref 34]*

# 3. Experimental Set-Up and Procedure

The main intention of this experimental work is to calculate the microcrack density at different stress levels in three different composite material systems. As described by Nairn [Ref 4], a logical experiment to characterize the microcracking properties of composite laminates is to follow the microcracking process and record the number of microcracks or microcracking density as a function of applied load. Hence our aim in this experimental work is to determine the microcrack density as a function of applied load.

There were three composite material systems investigated in the current study: IM7/977-2, IM7/5555 and IM7/5276-1. All these samples were cross-ply laminates of the [0/90/90/0] lay-up. From each composite panel six samples were tested until failure. The first aim of the experimental testing is to generate microcrack density for each composite. As noted by Nairn [Ref 5], microcracking density (here, noted in number of microcracks per centimeter) as a function of applied loading is necessary in determining the microcracking fracture toughness of the composites. This requires loading each sample to pre-determined stresses (whether it is the failure load or some high load preceding failure) at pre-determined stress intervals. A second objective is to analyze the microcracking progression. For each sample examined for this analysis, the procedure entailed finding the distance between each pair of adjacent cracks across the entire viewing span at each pre-determined stress level. Recall that in using the finite fracture mechanics approach for predicting microcrack progression, it is assumed that additional cracks always initiate at the center of the previous crack spacing. However, in practical applications this is not always the case. The current analysis is being performed to study the experimental

behavior in hopes of determining an *f* parameter (introduced by Nairn [Ref 5]) for each of the composites under investigation.

### 3.1 Material system

The carbon-epoxy cross ply composite panels which were used in the experimental work were made of three different resin systems and they have the same lay-up [90/0/0/90]. IM7/977-2, IM7/5555 and IM7/5276-1 are the panels which were used, where IM7 are the fibers and 977-2, 5555 and 5276-1 are the three different resin systems. 30 cm x 30 cm composite panels were manufactured by vacuum bagging at the Lockheed Martin Space Systems Company – Michoud Operations. Prior to cutting, these panels were tested via ultrasonic testing and concluded that they posses no initial damage. Each panel had four plies with [90/0/0/90] lay-up. The total thickness of the panels varied with IM7/977-2 being 0.55mm, IM7/5555 being 0.55 mm, and IM7/5276-1 being 0.60 mm.

### 3.2 Sample Preparation

Each panel was numbered and cut into four quadrants; each quadrant was numbered in a clockwise fashion beginning with the top right quadrant. This quadrant piece was cut further into four pieces and numbered in the same manner as before. These smaller pieces were then cut into samples measuring 60mm x 5mm. A typical numbering will look like 6-II-IV-1. Here the number 6 designates the IM7/5276-1 composite. II-IV-1 denotes the location that the sample was cut from the panel. This sample was the first one cut from the 3in by 3in quadrant IV section of the 6in by 6in quadrant II section. The panels are cut in such a manner that the final sample is cut along $0^o$ plies and $0^o$ plies are on the outer surface. The above dimensions are required for the

sample to accommodate the tensile substage. All cutting is performed with a circular diamond cutter at suitable speed with continuous flow of lubricant ensuring proper dimensions and heat removal. The blade of the cutter is a diamond metal bonded, wafer blade. *Table 3.1*, *Table3.2* and *Table 3.3* display the final dimensions and variation in these dimensions across the length of each sample tested.

***Table 3.1*** *Sample widths and variations for material system IM7/977-2*

| Sample | Width (mm) | Width (mm) | Difference (mm) | Final Width (mm) |
|---|---|---|---|---|
| 2-I-II-5 | 4.79 | 4.77 | 0.02 | 4.78 |
| 2-I-II-6 | 4.84 | 4.86 | 0.02 | 4.85 |
| 2-I-II-7 | 5.14 | 5.22 | 0.08 | 5.18 |
| 2-I-III-1 | 4.57 | 4.56 | 0.01 | 4.565 |
| 2-I-III-3 | 5.02 | 5.03 | 0.01 | 5.025 |
| 2-I-III-9 | 4.87 | 4.81 | 0.06 | 4.84 |

***Table 3.2*** *Sample widths and variations for Material System IM7/5555*

| Sample | Width (mm) | Width (mm) | Difference (mm) | Final Width (mm) |
|---|---|---|---|---|
| 5-I-II-1 | 4.57 | 4.55 | 0.02 | 4.56 |
| 5-I-II-2 | 4.84 | 4.82 | 0.02 | 4.83 |
| 5-I-II-3 | 4.88 | 4.92 | 0.04 | 4.90 |
| 5-I-II-5 | 4.95 | 4.97 | 0.02 | 4.96 |
| 5-I-IV-1 | 4.54 | 4.54 | 0.00 | 4.54 |
| 5-I-IV-3 | 4.77 | 4.64 | 0.13 | 4.76 |
| 5-I-IV-8 | 4.41 | 4.44 | 0.03 | 4.425 |
| 5-I-I-3 | 4.96 | 4.95 | 0.01 | 4.955 |

***Table 3.3*** *Sample widths and variations for Material System IM7/5276-1*

| Sample | Width (mm) | Width (mm) | Difference (mm) | Final Width (mm) |
|---|---|---|---|---|
| 6-II-IV-1 | 5.04 | 5.08 | 0.04 | 5.06 |
| 6-II-IV-2 | 4.75 | 4.78 | 0.03 | 4.765 |
| 6-II-IV-4 | 5.01 | 5.10 | 0.09 | 5.055 |
| 6-II-IV-5 | 4.78 | 4.75 | 0.03 | 4.765 |
| 6-II-IV-6 | 5.47 | 5.46 | 0.01 | 5..465 |
| 6-II-IV-7 | 4.98 | 5.01 | 0.03 | 4.995 |
| 6-II-IV-3 | 4.87 | 4.86 | 0.01 | 4.865 |

For preliminary tests, the side edge to be viewed was polished using a rotating polisher. However, better results for observing microcracking were obtained when P-2400 grit silicon carbide polishing paper was used to clean the edge surfaces of the sample to remove any adhesive, dust or foreign material after attaching the tabs (to be discussed in the next paragraph). An example of a microscopic photograph of a sample before testing (with no microcracks) is shown in *Figure 3.1*.

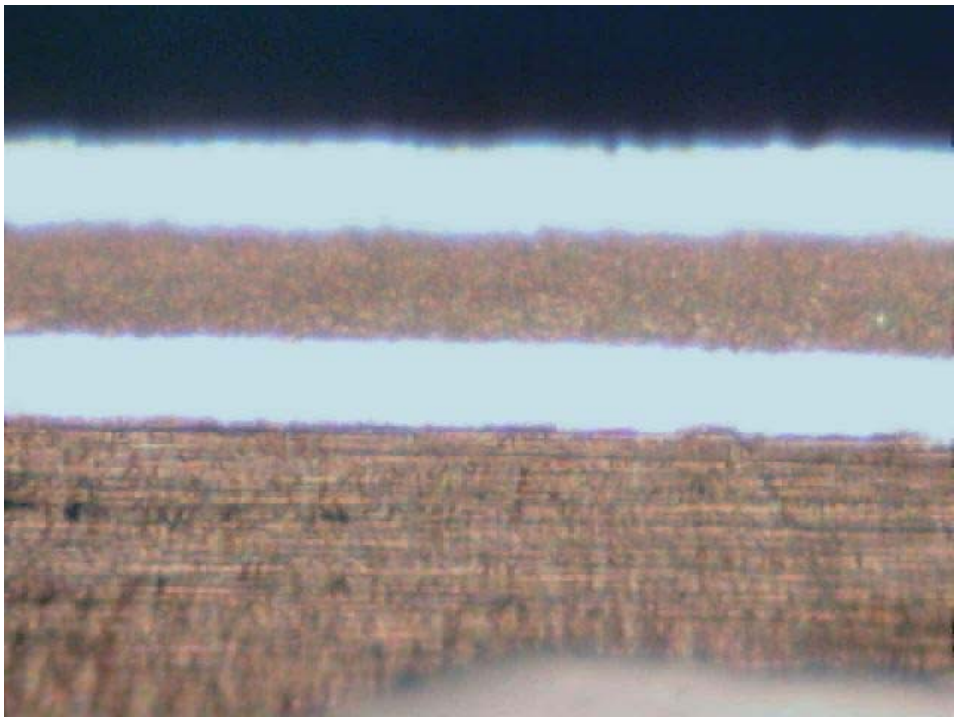

***Figure 3.1*** *Microscopic photograph of a sample before testing*

Before applying a tensile load, the samples were adhered with tabs on both sides at the ends. These tabs protect the sample from crushing because of the stress concentrations caused by the grip of the jaws and also these tabs provide a smooth gripping surface. Tabs distribute gripping stress and prevent them from crushing. These aluminum tabs are made of aluminum sheet of 20 gauge (0.80 mm) cut into approximately 10mm x 17mm pieces. The sample was glued using Loctite E-120HP Hysol epoxy adhesive. Before gluing the sample the surfaces of the sample and the aluminum tabs were made rough using 2-100 medium sand paper to ensure perfect bonding. The glue was mixed using a static mixer. An optimal quantity was used so that the glue itself does not fail under shear load. The glued sample was cured at room temperature up to 24 hours before testing. *Figure 3.2* shows four samples after preparation.

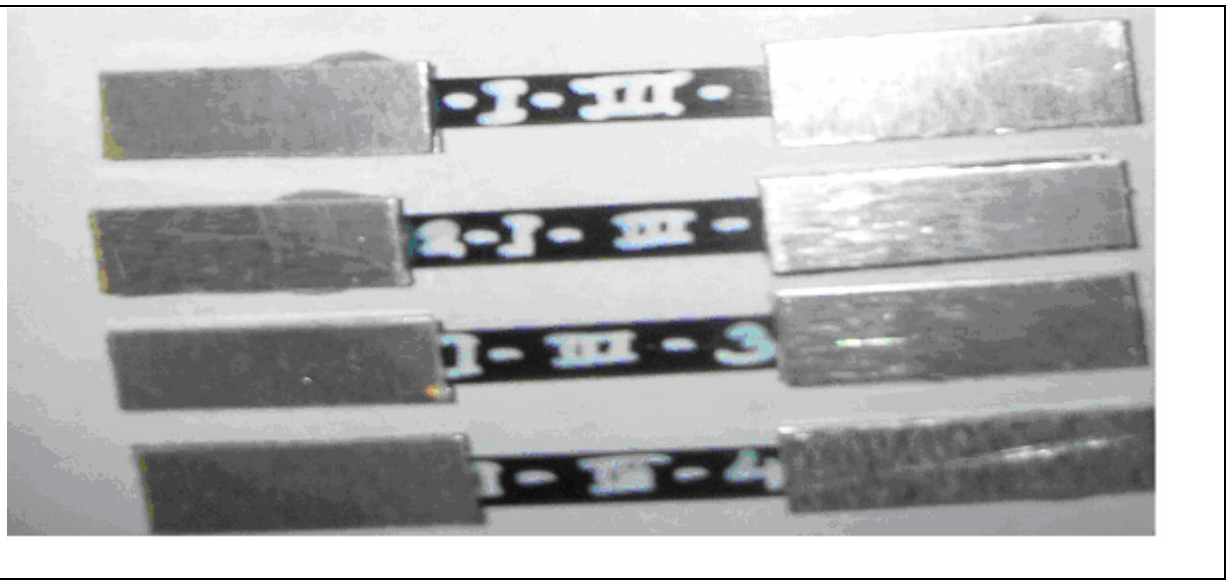

***Figure 3.2*** *Samples after preparation*

### 3.3 Experimental Set-up

Tensile testing was done using 2000 lb capacity tensile substage. The test setup comprises of a tensile substage, data acquisition system and mechanical testing software MTestWindows supplied by ADMET, Inc. *Figure 3.3* shows the experimental setup. *Figure 3.4* shows a close-up view of a sample in the substage.

***Figure 3.3*** *Experimental set-up*

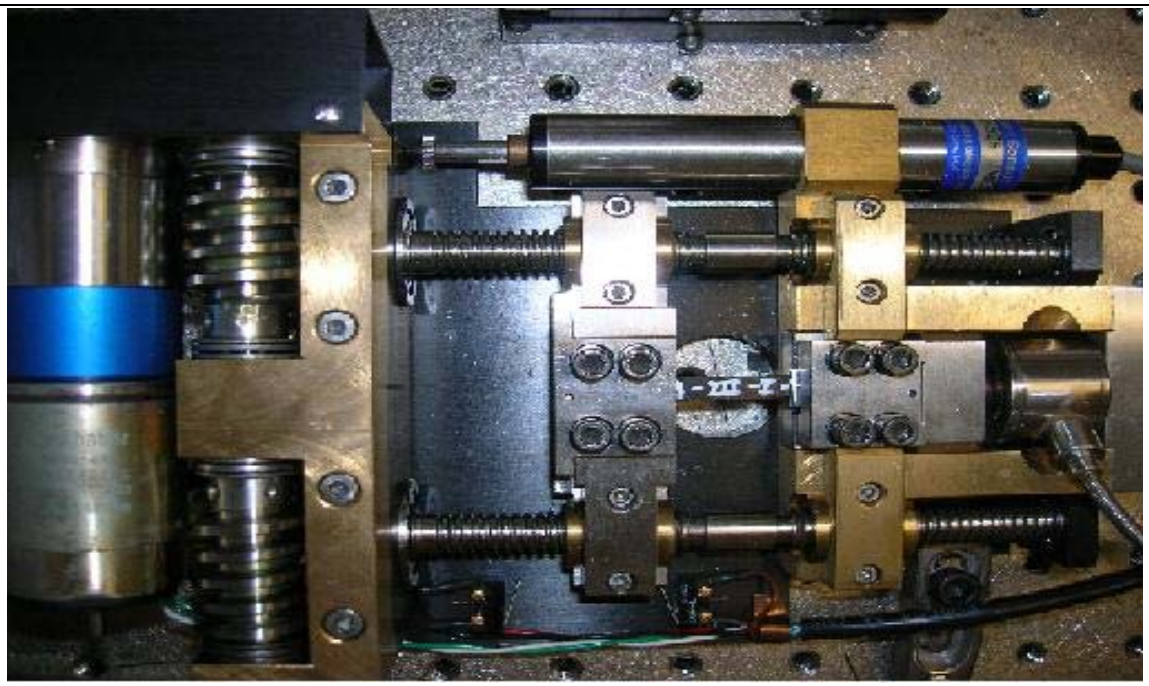

***Figure 3.4*** *Close-up view of a sample in the substage*

*Figure 3.5* depicts a typical screen of the software. This window displays five small windows on the screen; beginning from the top left in a clockwise order they are: the load on the sample, the stress, the displacement of the cross-heads, the strain and a load versus time graph. All windows display the live values, peak values, and rate of change in the parameter values at all times. Usually all the windows begin at zero except the displacement windows with some oscillating values at a third decimal place. Before beginning the test always it was noted to minimize the oscillation by clicking the zero button on the right hand side of the displacement window.

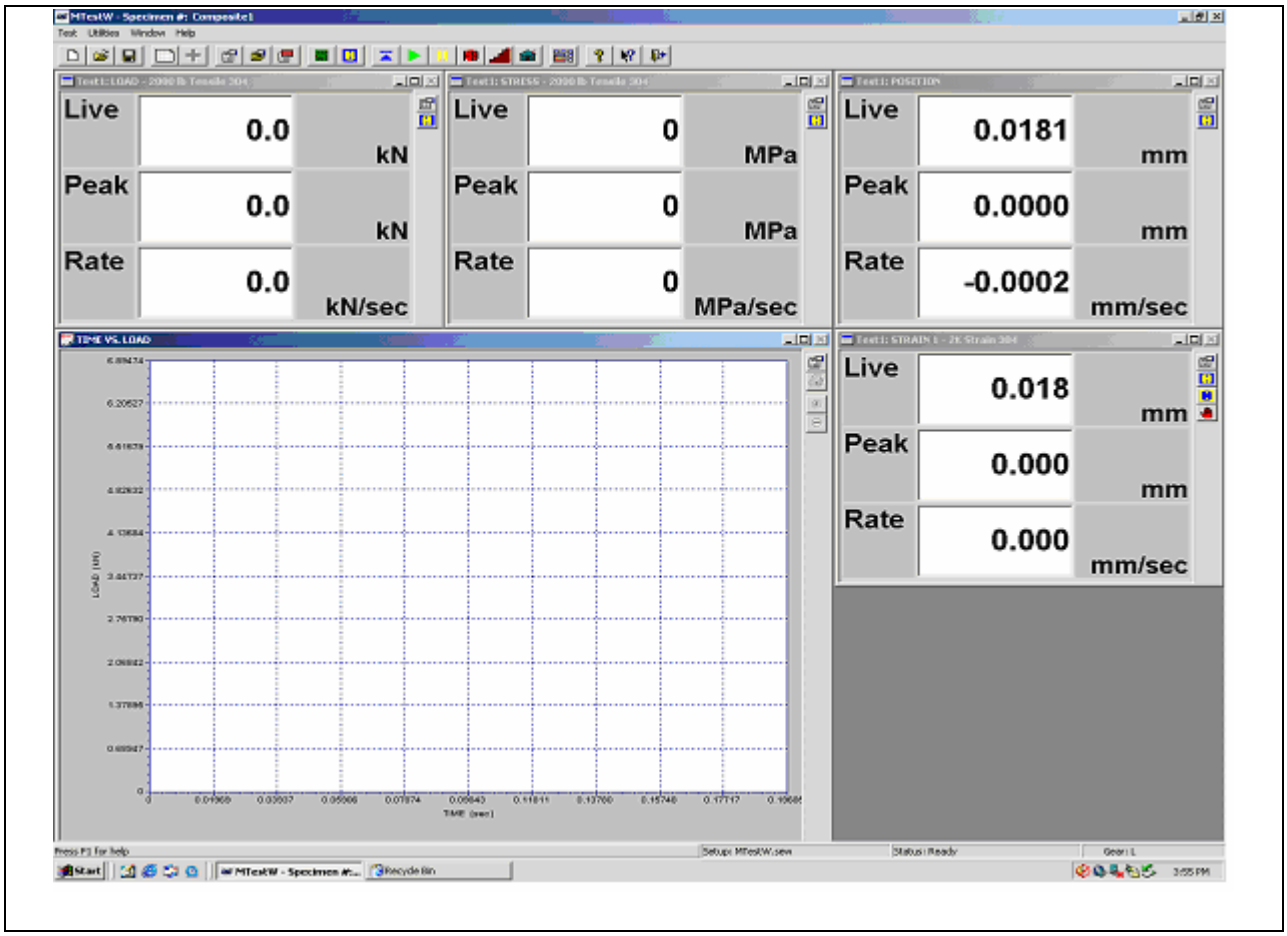


***Figure 3.5*** *Typical screen of the MTest Windows software*

A typical test setup menu is depicted in *Figure 3.6*. In the test setup window clicking on the display button gives options to display load, stress, length and time in desired units.

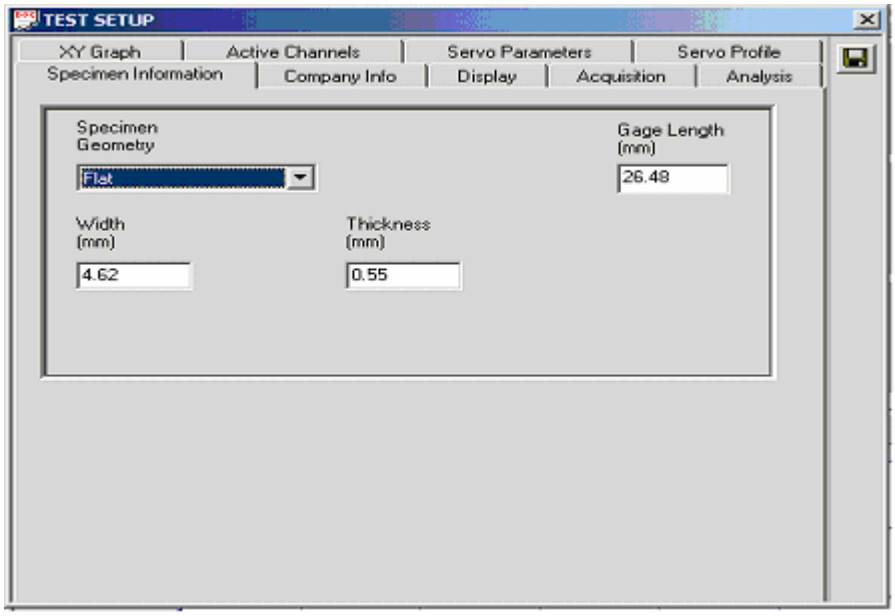


***Figure3.6*** *Screen shot of test set-up menu*

In the "servo parameters" option, as shown in *Figure 3.7*, the preload, preload rate, jog speed, home rate and the port test are fixed. The preload amount and the preload rate are used to apply small load to the sample prior to the starting of the test. This preload amount should be less than start test threshold. The jog speed is the rate at which the crosshead moves while loading the sample. The home rate is the rate at which the machine will return to its starting zero position when the home icon is clicked. Post test action defines the movement of the cross-head after the end of the test is detected. In the present testing, the stop option is selected for the post test action so as to not reverse load on the substage after testing; Very high loads could affect the load cells.

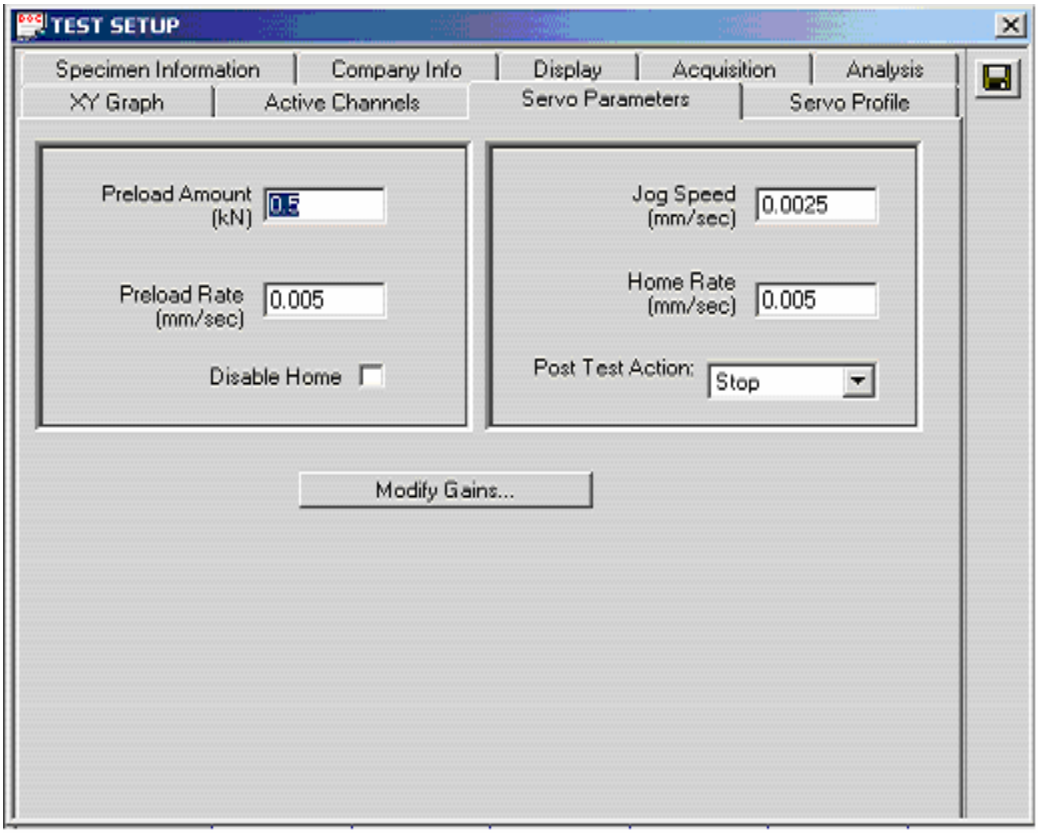


***Figure 3.7*** *Screen capture of servoparamaters Window*

The acquisition menu shown in *Figure 3.8* allows fixing parameters such as sample brake, threshold load and segmenting log rate. Sample brake is the load at which failure of the present sample is detected by the substage and to stop the testing. For the present test the sample break is set at 20% of the peak load of the sample. Threshold load is the load at which the program starts logging in data. The threshold rate should always be set higher then the preload. Finally, the segment log rate and segment duration defines the frequency and the length that the data is being logged. Most of the parameters are fixed and rarely change other then sample information and the servo-parameters.

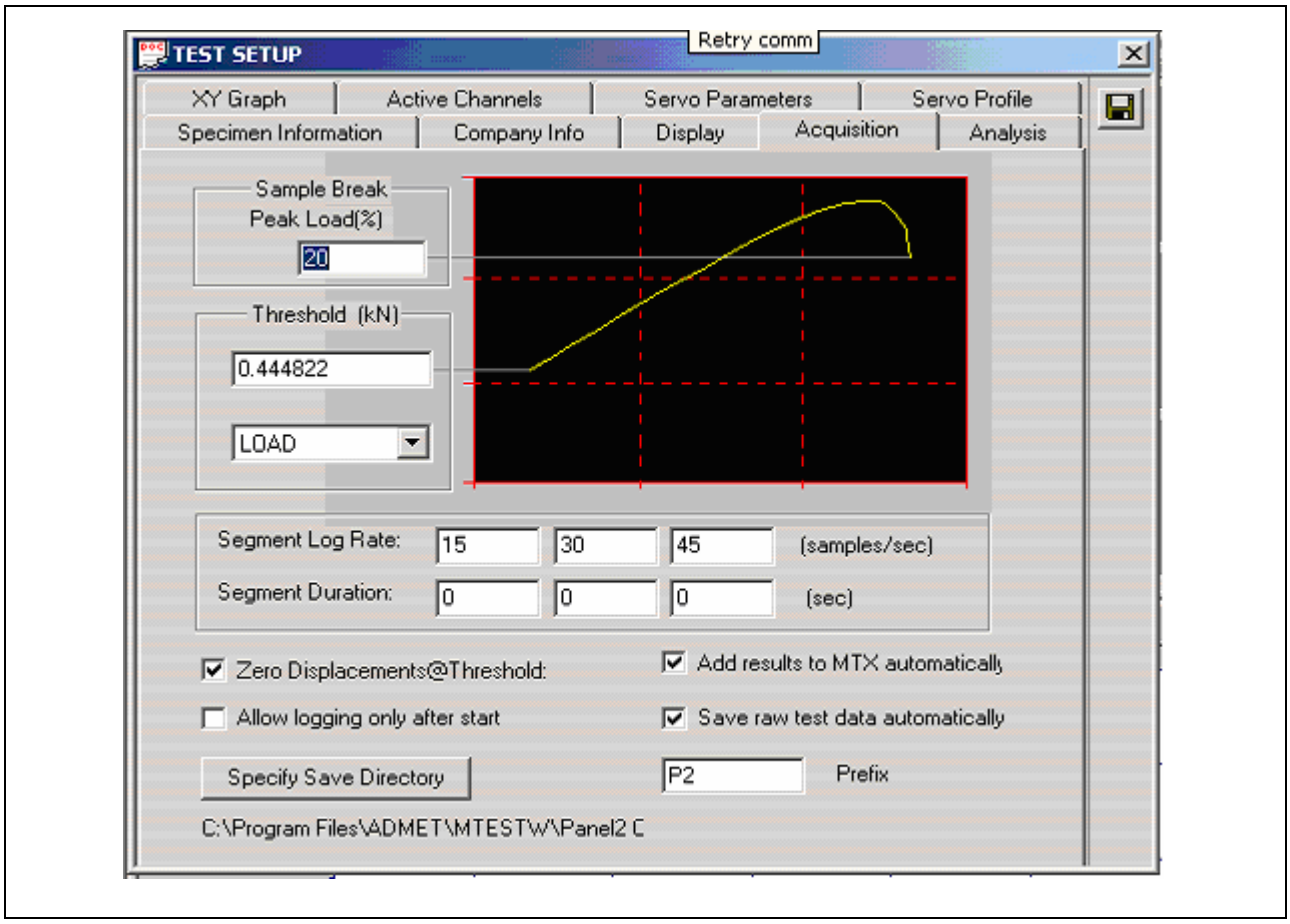


***Figure 3.8*** *Screen capture of acquisition menu*

### 3.4 Optical Microscopy

Optical microscopy was performed using a Pro-Scope digital USB microscope with a 200X magnification lens. The still capture capability of the microscope was 640x480 (VGA) pixels. The microscope was mounted on a stand parallel to the substage so as to focus on the surface developing microcracks. The stand of the microscope has a micrometer which facilitates 1) the movement of the microscope to and fro parallel to the surface under investigation and 2) the measurement of the distance moved. For the current testing, the typical in-focus span across the sample was between 10 mm to 14 mm. For clarity, this distance across the sample in which the micrographs are obtained will be referred to as the optical span length. A high intensity

illuminator was used to brighten the surface under investigation to get good results. *Figure 3.9* is a picture of the optical microscopy setup.

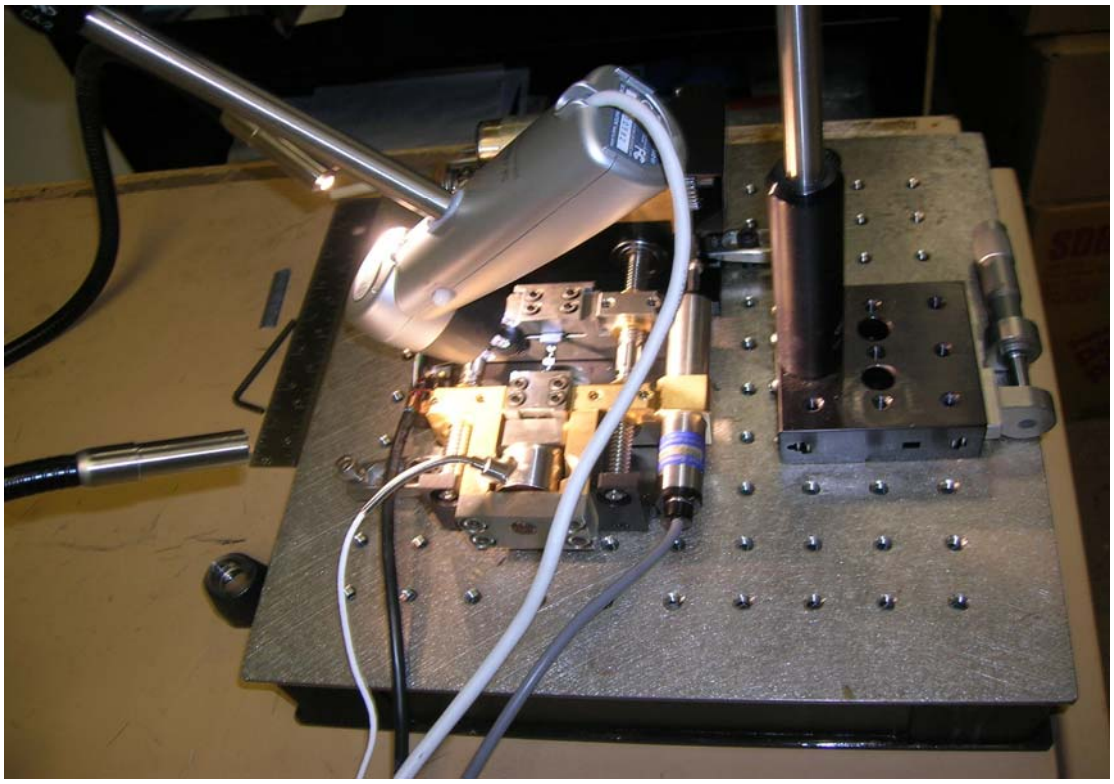

***Figure 3.9*** *Optical Microscope set-up*

### 3.5 Experimental Procedure

The acquisition system is turned on and it is made sure the acquisition system is in tension mode by using the switch on the data acquisition system. Then the Mtest Windows software is turned on.

The clamps of the substage are designed with two self adjusting wedge shaped grips to make a smooth tightening of the clamps. After the sample is placed between the clamps, they are hand-tightened and the distance between the clamps was measured using a digital caliper. This

distance is taken as the gauge length. For a typical sample the gauge length was around 25mm. Then the test setup icon is opened from the file pull-down menu in the MTest Windows software. The desired sample information is input using the sample information window. The parameters for the present testing used were flat sample, gauge length, width and thickness. After the sample information is entered the servoparameters are fixed. The servo-parameter settings for the present study is 0.0025 mm/sec for the jog speed, 0.005 mm/sec for the home rate, 0.5 KN for the preload, and the post test is set to stop.

The above test set-up is saved by the name of the sample and the screws of the clamps are tightened. After tightening the sample the stress and the load induced on the sample are noted to make sure the clamping stress and load not to exceed the preload.

Then the optical microscope is focused on the surface at one end and moved to the other end making a note of the span of focus of the microscope and best visualization of the surface throughout the sample. Then the sample is loaded, stopped at pre-determined stress intervals, and inspected using optical microscopy for microcracks. The samples in the present test are loaded to 800 MPa continuously as the micro cracking would not start until this load [Ref 2] and then stopped at every 50 MPa interval. At each of these loadings snap shots of the surface are taken. The field of view in each optical micrograph covers a 1.375mm sample length. After grabbing the first snap shot the micrometer is translated in increments of 1.25 mm until the total travel of the micrometer is between 10 and 14 mm (This length is dependent on the gauge length of the sample). An optical micrograph is taken at each increment of micrometer travel. A 10mm micrometer travel results in a total optical scan length of 11.375 mm.

### 3.6 Microcracks and Distance Measurements

As previously noted, the sample length in the field of view of a single micrograph is 1.375mm. Each of these images is captured with 640 horizontal and 480 vertical pixels. The snapshots from each stress level are grouped together and the number of microcracks for the optical scan length is counted. Note that this process is a bit tedious since there is an overlap length of 0.125mm between consecutive micrographs. Then by using a zooming software tool, ZoomMagic, the number of pixels between each crack is determined. *Figure 3.10* displays a typical optical micrograph and *Figure 3.11* displays the screen shot of the ZoomMagic software.

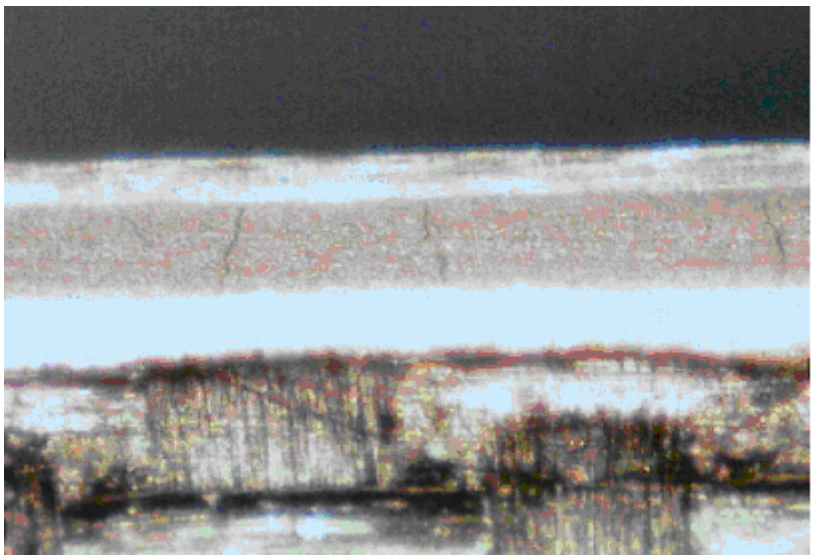

***Figure 3.10*** *Optical Micrograph*

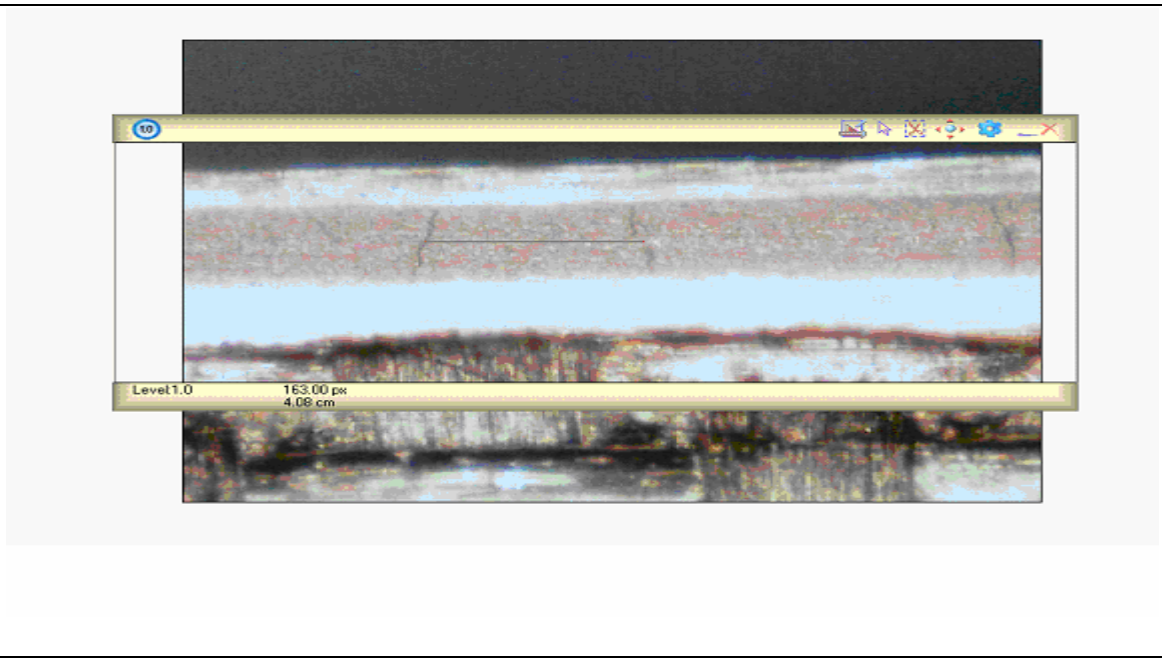


***Figure 3.11*** *Screen capture of Zoom-Magic software*

# 4. Results

The microcrack density as a function of applied stress was measured for the three composite material systems – IM7/977-2, IM7/5555 and IM7/5276-1. For each material system, at least six samples were tested. Optical microscopy was performed to determine the stress for microcrack initiation, propagation of microcrack density and individual microcrack. The data were analyzed using finite fracture mechanics and master-curve analysis to determine the microcracking fracture toughness for each material system.

## *4.1 Microcrack Density*

### *4.1.1 Material System IM7/977-2 [0/90]$_s$*

Six IM7/977-2 samples were tested on the tensile substage shown in *Figure 3.4* and microscopy was performed to record the data required to calculate microcrack density, as described in Section 3.6. A typical microscopic photograph is shown in *Figure 4.1*. Here two microcracks can be seen. The distance between microcracks is measured using the ZoomMagic software package as explained in Chapter 3.

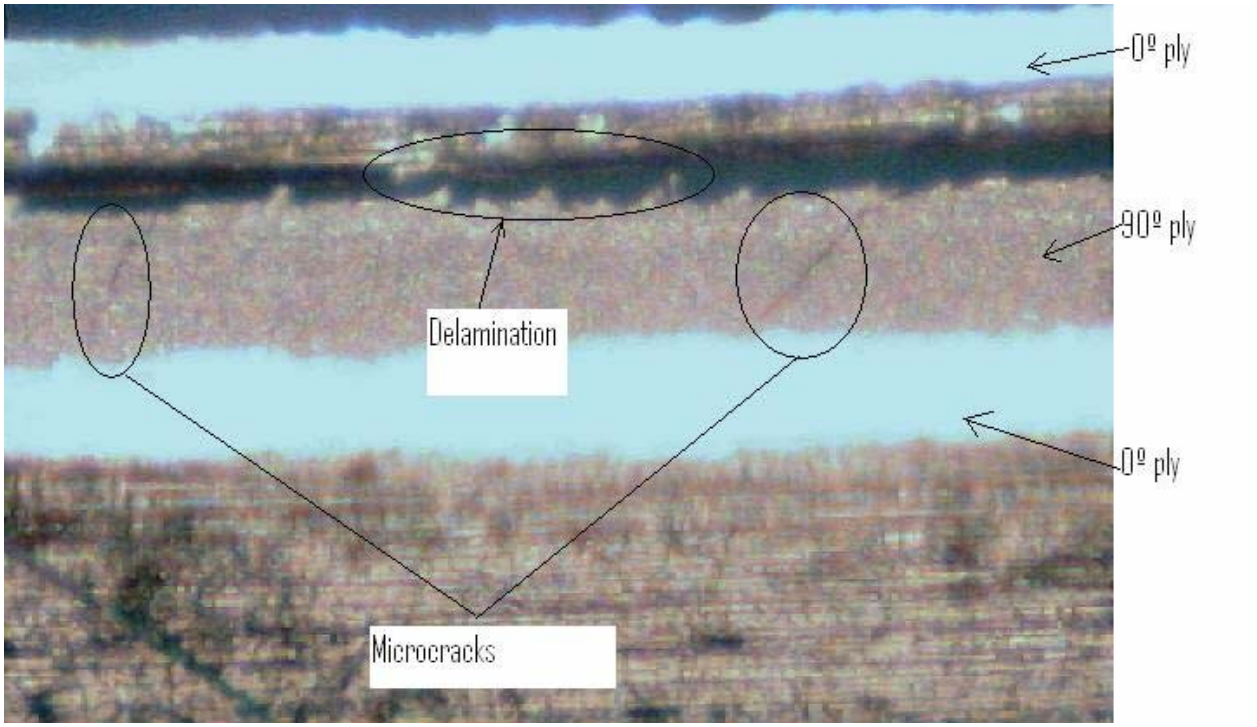


***Figure 4.1*** *A typical picture obtained from Microscopy*

*Table 4.1* lists the crack densities ($m^{-1}$) at applied stress (MPa) for each sample. In *Table 4.1* we can see that the first microcrack was observed at around 1000-1050 MPa and beyond this point the microcracks increased with the applied stress. The maximum crack density was measured at the stress level below the failure stress. The crack density at the failure stress was not measured as the sample broke at that stress.

***Table 4.1*** *Crack densities (D in $m^{-1}$) at applied stress (σ in MPa) for each sample of the material system IM7/977-2*

| **2-I-III-1** | | **2-I-III-3** | | **2-I-II-6** | | **2-I-II-7** | | **2-I-III-9** | | **2-I-II-5** | |
|---|---|---|---|---|---|---|---|---|---|---|---|
| **σ** | **D** | **σ** | **D** | **σ** | **D** | **σ** | **D** | **σ** | **D** | **σ** | **D** |
| 1054 | 72.07 | 1026 | 615.38 | 1015 | 87.91 | 1005 | 87.91 | 1065 | 197.53 | 960 | 98.765 |
| 1107 | 144.14 | 1079 | 879.12 | 1056 | 351.65 | 1050 | 175.82 | 1113 | 197.53 | 1029 | 197.53 |
| 1178 | 144.14 | 1120 | 967.03 | 1118 | 439.56 | 1098 | 263.74 | 1160 | 592.59 | 1133 | Failed |
| 1222 | 432.43 | 1172 | 1054.95 | 1185 | 791.20 | 1148 | 263.74 | 1180 | Failed | | |
| 1256 | 504.50 | 1208 | Failed | 1222 | Failed | 1204 | 439.56 | | | | |
| 1297 | 1153.15 | | | | | 1250 | 615.38 | | | | |
| 1322 | Failed | | | | | 1266 | Failed | | | | |

*Figure 4.2*, a plot of the microcrack density as a function of the applied stress, illustrates the micro crack propagation with the applied stress for IM7/977-2 material system.

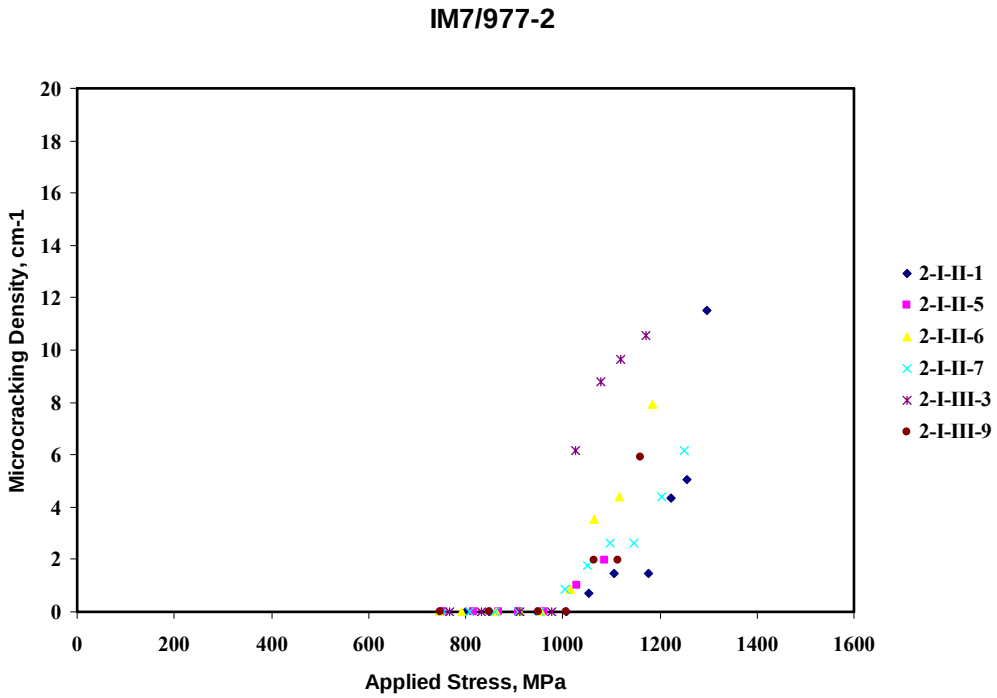


***Figure 4.2*** *Microcrack density vs. Stress plot for* $[0/90]_s$ *IM7/977-2*

*Table 4.2* lists the optical scan length, the crack initiation stress, the maximum stress (failure stress) induced in the sample and the maximum crack density. The optical scan length for all the material systems was about 10-14 mm. The gauge length, the length of the sample between the two jaws of the tensile stage, was between 23-25 mm. Microcrack density is calculated by dividing the number of microcracks formed by the length of the region in which they were observed. This microcrack density is very crucial in determining the fracture toughness and this will be illustrated in further sections of this chapter.

***Table 4.2*** *Microcracking and load data for material system IM7/977-2*

| Sample | Optical Span Length (mm) | Crack Initiation Stress (MPa) | Crack Density (Cracks/cm) | Maximum Stress (MPa ) |
|---|---|---|---|---|
| 2-I-II-5 | 10.125 | 960 | 2.0 | 1133 |
| 2-I-II-6 | 11.375 | 1015 | 7.9 | 1222 |
| 2-I-II-7 | 11.375 | 1005 | 6.2 | 1266 |
| 2-I-III-1 | 13.875 | 1054 | 11.53 | 1322 |
| 2-I-III-3 | 11.375 | 1026 | 10.5 | 1208 |
| 2-I-III-9 | 10.125 | 1065 | 5.9 | 1180 |

*Figure 4.3* and *Figure 4.4* depict schematics of the typical crack formation in IM7/977-2 samples with applied stress. From the schematics it can be seen that the microcracks did not initiate in the mid span of the optical scan of the sample. After the initial formation, new cracks initiated between the existing microcracks. The maximum number of 16 cracks was observed in sample 2-I-III-1 at 1296 MPa for an observable span of 13.875 mm, which resulted in a crack density of 11.5 cracks/cm. This material system did not show a clear indication of microcracking saturation. This is may be due the fact that at higher loads the energy was released due to other forms of damage, such as delamination, fiber pull-out, etc

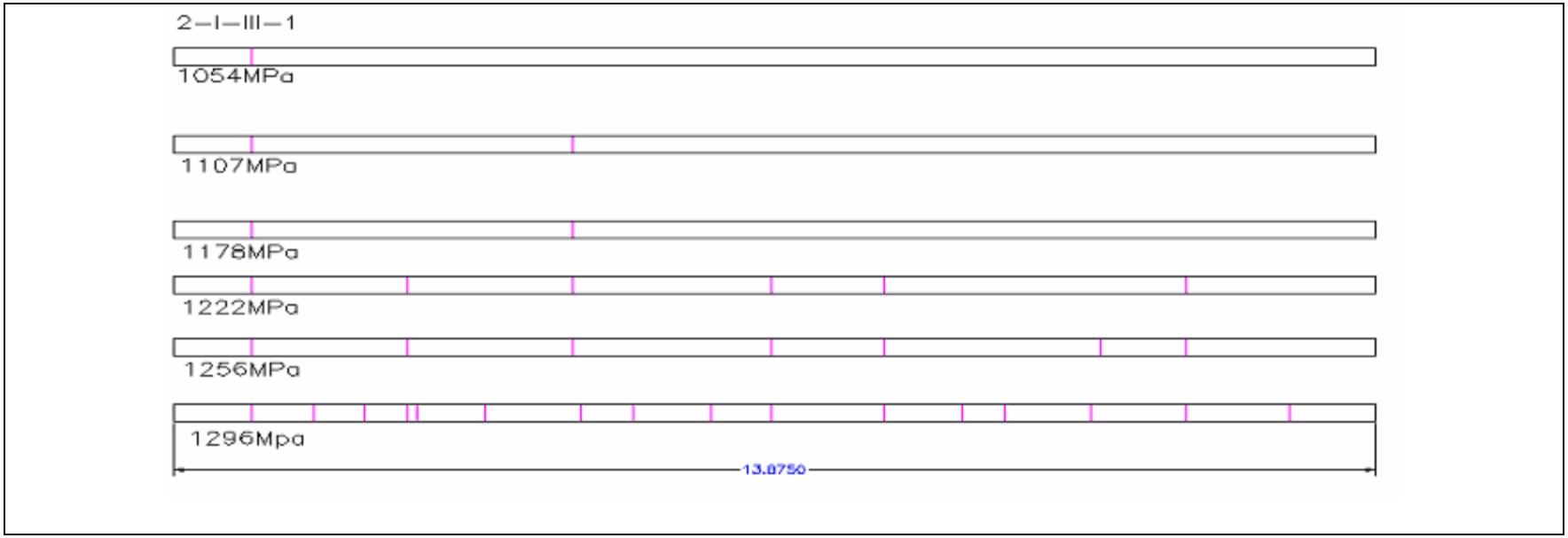


***Figure 4.3*** *Schematics of crack propagation in IM7/977-2 sample 2-I-III-1[Ref 37]*

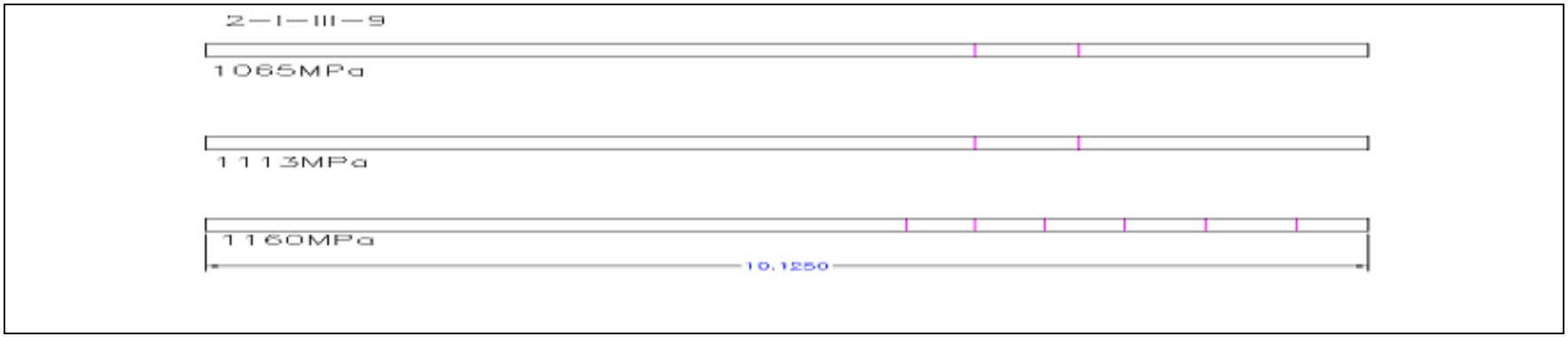


***Figure 4.4*** *Schematics of crack propagation in IM7/977-2 sample 2-I-III-9 [Ref 37]*

### *4.1.2 Material System IM7/5555 $[0/90]_s$*

A total of six samples from IM7/5555 were tested on the tensile substage shown in *Figure 3.4* and microscopy was performed to record the data required to calculate microcrack density. *Table 4.3* lists the crack densities ($m^{-1}$) at applied stress (MPa) for each sample. In *Table 4.3* we can see that the first microcrack was observed at around 850 MPa and beyond this point the microcracks increased with the applied stress. The maximum crack density measured was at the stress level below the failure stress. The crack density at the failure stress was not measured as the sample broke at that stress. The IM7/5555 material system failed at higher loads than that of IM7/977-2 but the crack initiation was at lower loads than that of IM7/977-2. The average failure stress for the six samples tested to failure was found to be around 1330 MPa.

***Table 4.3*** *Crack densities (D in $m^{-1}$) at applied stress (σ in MPa) for each sample of the material system IM7/5555*

| **5-I-II-1** | | **5-I-II-2** | | **5-I-II-3** | | **5-I-II-5** | | **5-I-IV-1** | | **5-I-IV-3** | |
|---|---|---|---|---|---|---|---|---|---|---|---|
| **σ** | **D** | **σ** | **D** | **σ** | **D** | **σ** | **D** | **σ** | **D** | **σ** | **D** |
| 871 | 263.74 | 876 | 527.47 | 893 | 87.91 | 922 | 87.91 | 818 | 175.82 | 855 | 175.82 |
| 925 | 351.65 | 934 | 791.20 | 977 | 87.91 | 964 | 87.91 | 871 | 175.82 | 902 | 175.82 |
| 982 | 351.65 | 984 | 967.03 | 1033 | 351.65 | 1016 | 263.74 | 922 | 351.65 | 970 | 439.56 |
| 1040 | 527.47 | 1021 | 1054.94 | 1081 | 879.12 | 1071 | 263.74 | 974 | 439.56 | 1025 | 439.56 |
| 1097 | 879.12 | 1064 | 1142.86 | 1127 | 1142.86 | 1114 | 439.56 | 1020 | 527.47 | 1080 | 615.38 |
| 1152 | 967.03 | 1111 | 1230.77 | 1185 | 1218.68 | 1153 | 527.47 | 1062 | 615.38 | 1147 | 1230.77 |
| 1206 | 1054.95 | 1147 | 1318.68 | 1238 | 1406.59 | 1199 | 615.38 | 1190 | 791.20 | 1205 | 1318.68 |
| 1206 | Failed | 1199 | 1494.50 | 1352 | Failed | 1270 | 703.30 | 1171 | 1142.86 | 1252 | 1494.50 |
| | | 1252 | 1670.33 | | | 1323 | 1054.95 | 1216 | 1318.68 | 1304 | 1670.33 |
| | | 1316 | 1670.33 | | | 1369 | 1494.50 | 1263 | 1670.33 | 1344 | Failed |
| | | 1316 | Failed | | | 1425 | 1494.50 | 1311 | 1670.33 | | |
| | | | | | | 1475 | 1670.33 | 1311 | Failed | | |
| | | | | | | 1495 | 1670.33 | | | | |
| | | | | | | 1495 | Failed | | | | |

*Figure 4.5*, a plot of the microcrack density as a function of the applied stress, illustrates the micro crack propagation with the applied stress for IM7/5555 material system.

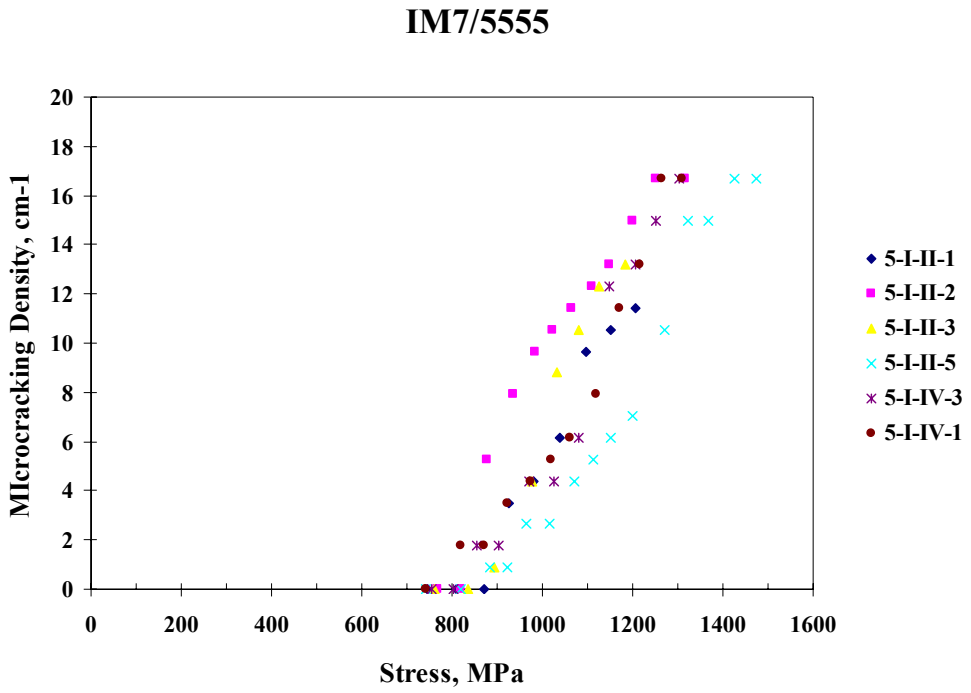


***Figure 4.5*** *Microcrack density vs. Stress plot for* $[0/90]_s$ *IM7/5555*

*Table 4.4* lists the optical scan length, the crack initiation stress, the maximum stress induced in the sample, and the maximum crack density for the IM7/5555 samples. As can be seen from *Table 4.4*, five of the samples reached a crack density of 16.7 cracks/cm. It can also be noted that sample groups 5-I-IV-1, 5-I-IV-3 and 5-I-II-2, 5-I-II-5 were cut from the same location of the initial panel and they all reached the same crack density. For the six samples loaded up to failure the average crack density at failure was found to be 15.2 cracks/cm. In this material system microcrack initiation was observed at around the load of 850 MPa.

***Table 4.4*** *Microcracking and load data for material system IM7/5555*

| Sample | Optical scan length (mm) | Crack Initiation Stress (MPa) | Crack Density (Crack/cm) | Maximum Stress ( MPa ) |
|---|---|---|---|---|
| 5-I-II-1 | 11.375 | 871 | 10.54 | 1206 |
| 5-I-II-2 | 11.375 | 876 | 16.7 | 1316 |
| 5-I-II-3 | 11.375 | 893 | 14.06 | 1352 |
| 5-I-II-5 | 11.375 | 884 | 16.7 | 1495 |
| 5-I-IV-1 | 11.375 | 818 | 16.7 | 1311 |
| 5-I-IV-3 | 11.375 | 855 | 16.7 | 1304 |

*Figure 4.6* and *Figure 4.7* depict schematics of the typical crack formation in IM7/5555 samples with applied stress.

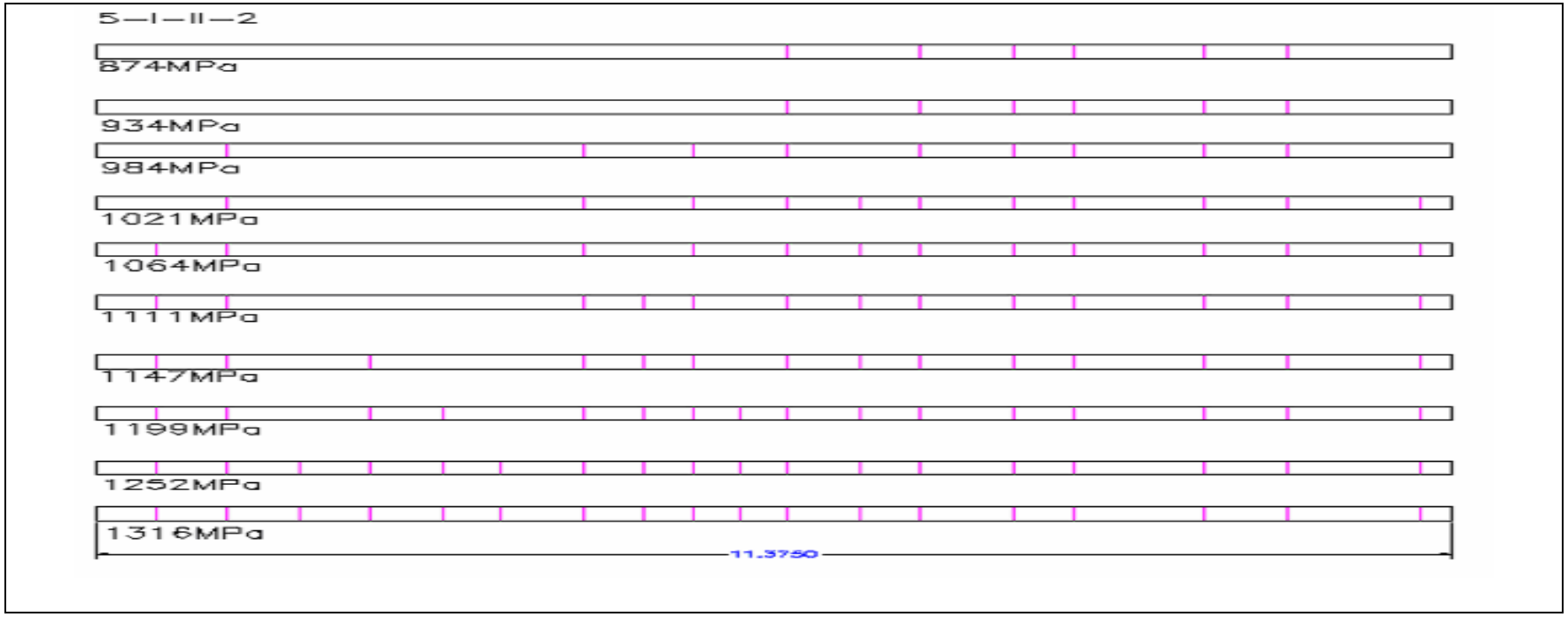


***Figure 4.6*** *Schematic of crack propagation in sample 5-I-II-2 [Ref 37]*

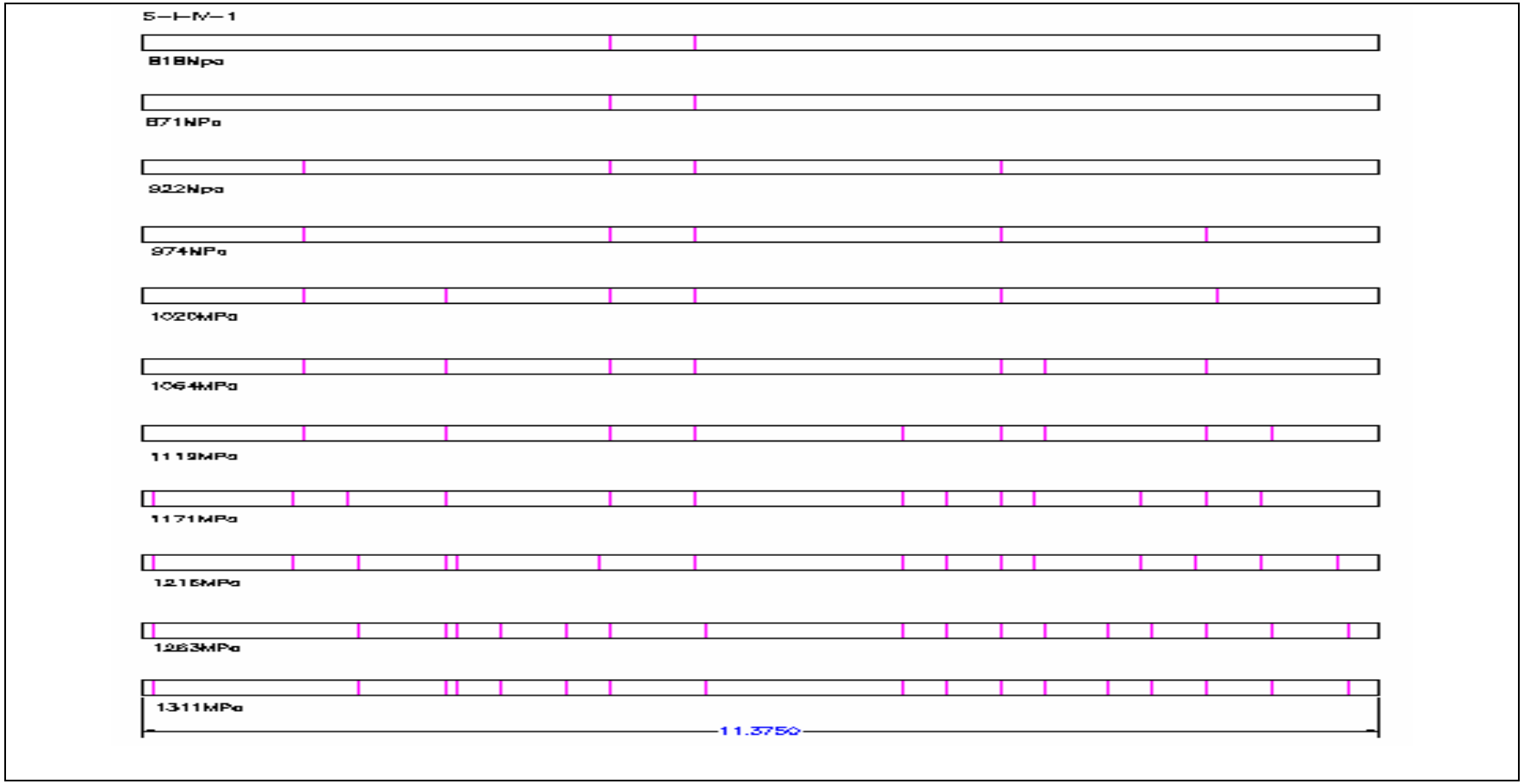


***Figure 4.7*** *Schematic of crack propagation in sample 5-I-IV-1 [Ref 37]*

For the material system IM7/5555 all the samples had an equal optical span length of 11.375 mm and it can also be observed from *Figure 4.6* and *Figure 4.7* that the microcraking has started in the mid-span of the sample, as expected. A majority of the samples, 4 of 6, displayed the same number of microcracks resulting in a crack density of 16.7 cracks/cm. The cracks were more evenly distributed throughout the length of the samples than those of the IM7/977-2 samples.

### *4.1.3 Material System IM7/5276-1 $[0/90]_s$*

Seven samples from IM7/5276-1 were tested using the tensile substage shown in *Figure3.4* and microscopy was performed to record the data required to calculate microcrack density. *Table 4.5* lists the crack densities ($m^{-1}$) at applied stress (MPa) for each sample. In *Table 4.5* we can see that the first microcrack was observed at around 950 MPa and beyond this point the microcracks increased with the applied stress. The maximum crack density measured was at the stress level below the failure stress. The crack density at the failure stress was not measured as the sample broke at that stress. IM7/5276-1 material system also failed at higher loads than that of IM7/977-2 but the crack initiation was at lower loads than that of IM7/977-2.

***Table 4.5*** *Crack densities (D in $m^{-1}$) at applied stress (σ in MPa) for each sample of the material system IM7/5276-1*

| **6-II-IV-1** | | **6-II-IV-2** | | **6-II-IV-3** | | **6-II-IV-4** | | **6-II-IV-5** | | **6-II-IV-6** | | **6-II-IV-7** | |
|---|---|---|---|---|---|---|---|---|---|---|---|---|---|
| **σ** | **D** | **σ** | **D** | **σ** | **D** | **σ** | **D** | **σ** | **D** | **σ** | **D** | **σ** | **D** |
| 932 | 296.29 | 1004 | 98.76 | 950 | 197.53 | 1010 | 197.53 | 983 | 98.76 | 870 | 263.74 | 751 | 72.07 |
| 981 | 296.29 | 1056 | 296.29 | 1017 | 395.06 | 1057 | 296.29 | 1015 | 395.06 | 926 | 351.65 | 801 | 216.21 |
| 1023 | 395.06 | 1102 | 296.29 | 1063 | 493.83 | 1106 | 395.06 | 1075 | 691.36 | 973 | 351.65 | 852 | 288.28 |
| 1080 | 493.83 | 1162 | 395.06 | 1127 | 691.35 | 1161 | 592.59 | 1118 | 888.89 | 1026 | 439.56 | 970 | 432.43 |
| 1128 | 493.83 | 1199 | 592.60 | 1166 | 790.12 | 1208 | 888.89 | 1152 | 1086.42 | 1073 | 615.38 | 1024 | 504.50 |
| 1181 | 790.12 | 1256 | 691.35 | 1217 | 987.65 | 1255 | 888.89 | 1208 | 1086.42 | 1108 | 879.12 | 1076 | 720.72 |
| 1231 | 888.89 | 1301 | 790.12 | 1255 | 987.65 | 1307 | 987.65 | 1265 | 1185.18 | 1162 | 967.03 | 1123 | 792.79 |
| 1278 | 888.89 | 1345 | 790.12 | 1310 | 1086.42 | 1358 | 1283.95 | 1295 | 1382.72 | 1202 | 1142.86 | 1160 | 1009 |
| | | | | 1357 | Failed | 1381 | Failed | 1349 | 1481.48 | 1202 | Failed | 1160 | Failed |

*Figure 4.8*, a plot of the microcrack density as a function of the applied stress, illustrates the micro crack propagation with the applied stress for IM7/5276-1 material system

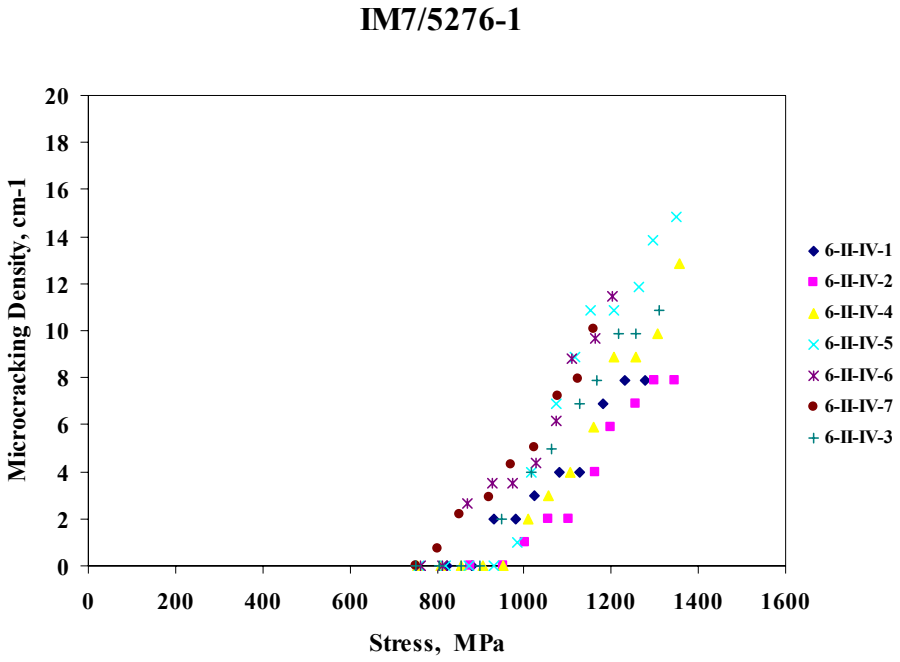


***Figure 4.8*** *Microcrack density vs. Stress plot for* $[0/90]_s$ *IM7/5276-1*

*Table 4.6* lists the optical scan length, the crack initiation stress, the maximum stress induced in the sample, the maximum crack density for the IM7/5276-1 samples.

***Table 4.6*** *Microcracking and load data for material system IM7/5276-1*

| Sample | Optical scan length (mm) | Crack Initiation load (MPa) | Crack Saturation Density ( Cracks/cm) | Maximum Stress(MPa ) |
|---|---|---|---|---|
| 6-II-IV-1 | 10.125 | 932 | 8.8 | 1278 |
| 6-II-IV-2 | 10.125 | 1004 | 7.9 | 1345 |
| 6-II-IV-4 | 10.125 | 1010 | 12.8 | 1381 |
| 6-II-IV-5 | 11.375 | 983 | 14.8 | 1349 |
| 6-II-IV-6 | 11.375 | 870 | 11.4 | 1202 |
| 6-II-IV-7 | 13.875 | 852 | 10.1 | 1160 |
| 6-II-IV-3 | 10.125 | 950 | 10.9 | 1357 |

From *Table 4.6* it is evident that, except for samples 1 and 2, the samples went up to a high crack density. *Figure 4.9* and *Figure 4.10* depict schematics of a typical crack formation in IM7/5276-1 samples with applied stress.

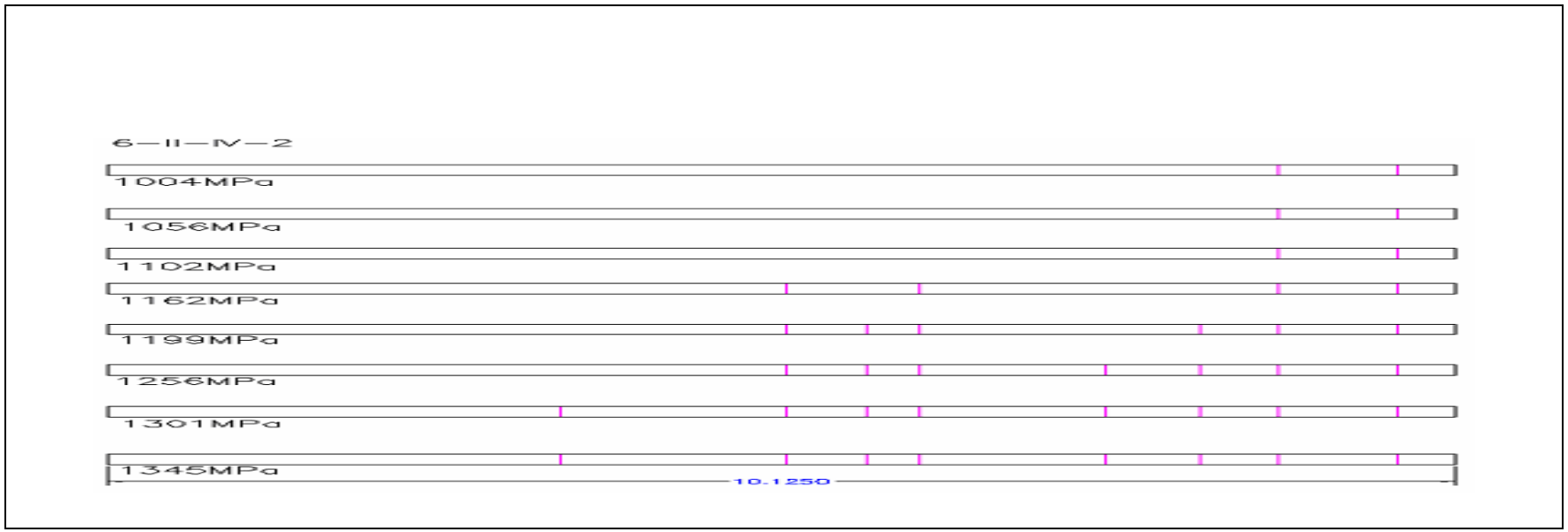


***Figure 4.9*** *Schematics of crack propagation in sample 6-II-IV-2 [Ref 37]*

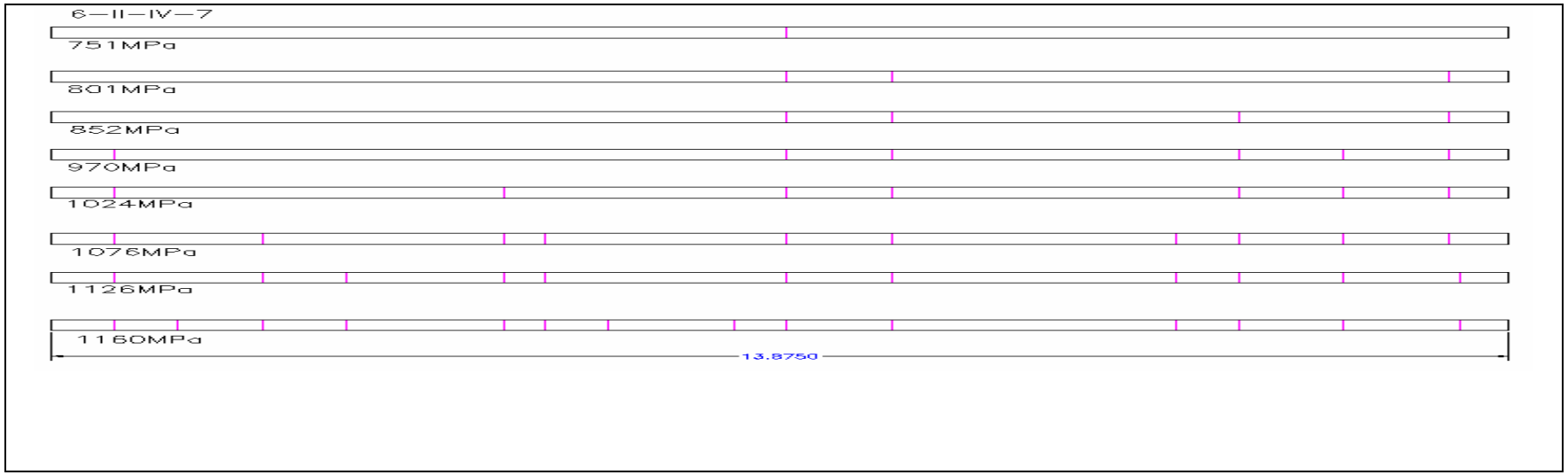


***Figure 4.10*** *Schematics of crack propagation sample 6-II-IV-7 [Ref 37]*

## *4.2 Finite Fracture Mechanics and Master-Curve Analysis*

As described in the previous chapters, the microcracking fracture toughness, $G_{m,}$ is a useful material property in determining the microcraking initiation and progress under a uni-axial loading.

### *4.2.1 IM7/977-2*

Material properties of the material system IM7/977-2 are listed in *Table 4.7* and the microcracking fracture toughness is calculated using the finite fracture mechanics and master-curve plot.

***Table 4.7*** *Input material properties for IM7/977-2*

| **Property** | **Value** |
|---|---|
| $E_a$ ( Axial Modulus ply material ) | 159 GPa |
| $E_t$ ( Transverse Modulus of ply material ) | 9.2 GPa |
| $E_c$ (x- direction modulus of cross-ply laminate) | 84.2 GPa |
| $G_a$ (Axial Shear modulus) | 4.37 GPa |
| $G_t$ (Transverse Shear modulus) | 2.57 GPa |
| $\alpha_a$ (Axial thermal expansion coefficient ) | -0.09 ppm/$^o$C |
| $\alpha_t$ (Transverse thermal expansion coefficient) | 28.8 ppm/$^o$C |
| $v_a$ ( Axial Poisson's Ratio) | 0.253 |
| $v_t$ ( Transverse Poisson's Ratio) | 0.456 |
| $T_{eff}$ ( Stress free temperature) | -125 $^o$C |

Of the above properties in *Table 4.7*, $E_a$, $E_c$, $E_t$, $G_a$, $G_t$, $v_a$ and $v_t$ were provided by the manufacturer of the samples, Lockheed Martin Corporation and $\alpha_a$ and $\alpha_t$ values were taken from Ref [4] as they are common for most graphite/epoxy material systems. $T_{eff}$, the stress-free temperature, is basically the difference between the curing temperature (177°C) and room temperature (24°C). To account for the possibility of some relaxation at high temperatures $T_{eff}$ is taken to be -125°C. The ply thickness of 0.1375mm was also provided by the manufacturer. After accumulating these properties the only required inputs were the crack spacing and the crack density, *D*, at each stress level. A small program has been written in Microsoft Excel to find the microcracking fracture toughness using the equations specified in Chapter 2 and a screen capture of the program is shown in *Figure 4.11*.

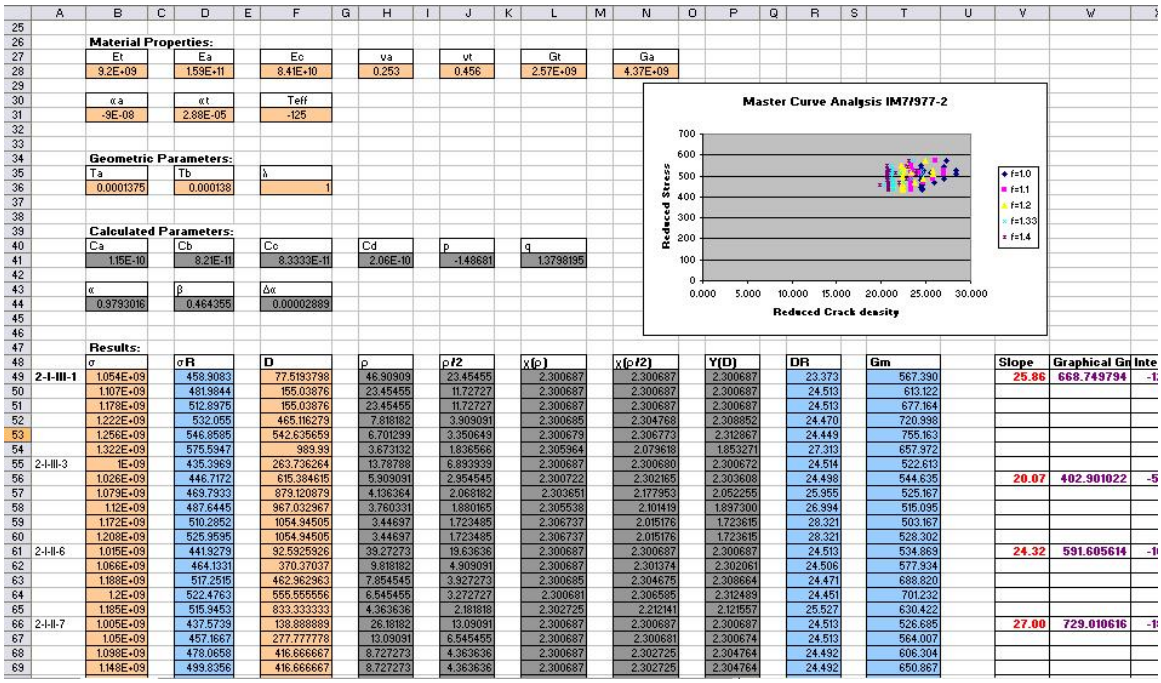


***Figure 4.11*** *Screen capture of the spreadsheet used to calculate the microcraking fracture toughness, Gm, and also to plot the master-curve*

The spread sheet has been designed such that once all the required material properties have been entered then the only required values are crack density, D, and the stress at which the crack density has been measured. The last column in the spreadsheet gives the fracture toughness, Gm, calculated by using equation (18), mentioned in the literature review, Chapter 2, of this work. The master curve plot for material system is shown in *Figure 4.12*.

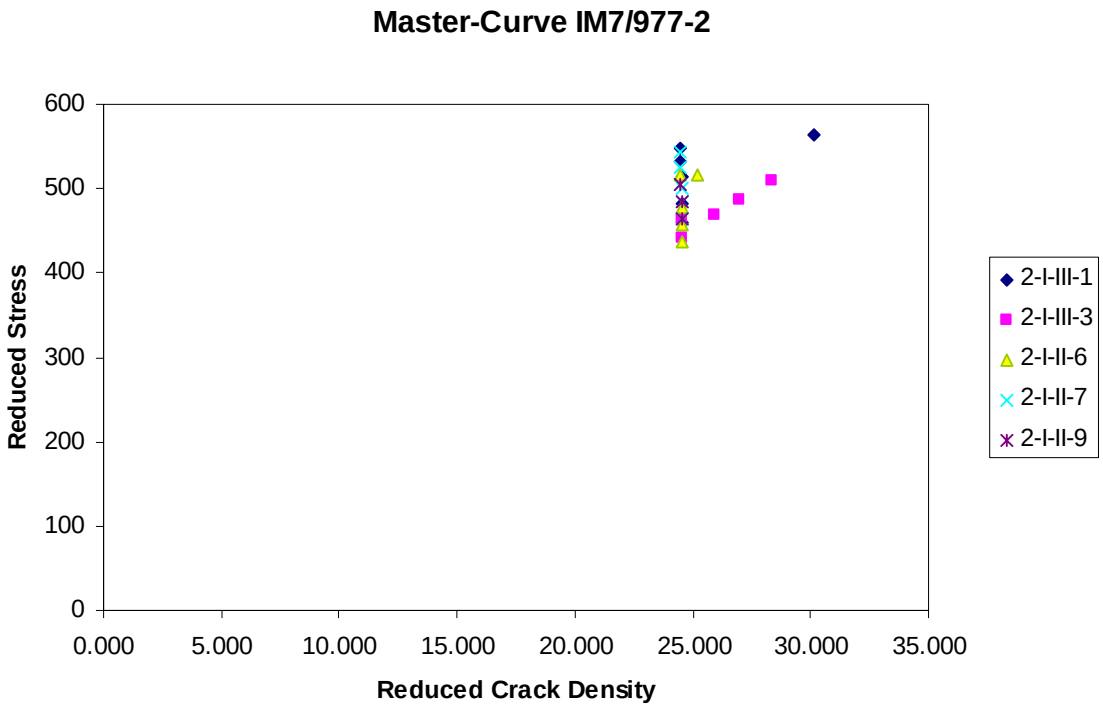


***Figure 4.12*** *Master plot for $[0/90]_s$, IM7/977-2 laminate*

The master curve is a plot of reduced crack density against reduced stress, the equations are provided in Chapter 2. The square of the slope of that curve gives the value of microcracking fracture toughness, Gm, and the intercept of the plot gives the value of $T_{eff}$. Average value of the microcracking fracture toughness for material system IM7/977-2 from the finite fracture mechanics using the equations described in Chapter 2 is found to be 610 $J/m^2$. From *Figure*

*4.12* it can be seen that most of the data points are in a vertical line. This is called the low crack density regime [Ref 34]. While performing master curve analysis the low crack density regime is neglected. Also, a parameter '*f*' plays a significant role in determining the microcracking fracture toughness at high crack densities using master plot. The parameter *f* represents the average ratio of the size of the crack interval in which a microcrack forms to the average crack spacing [Ref.5].

Several methods were reported in previous studies [Ref 5, 34] to determine values for *f*. One is to determine the average $\chi(\rho)$ at each crack density and compare it to calculated values. To facilitate this, the complete distribution of crack spacings was measured at each stress level for each sample. The values of $\chi(\rho)$ at each crack spacing, $a_i$, (where *i* goes from *1* to *n*, with *n* being the total number of crack spacings) was calculated and the average vale of $\chi(\rho)$ was plotted as function of crack density. The results are depicted in *Figure 4.13*. In this plot the solid lines represent the theoretical curves calculated for various values of *f*. These were calculated following the methods described by Nairn et al. [Ref 34].

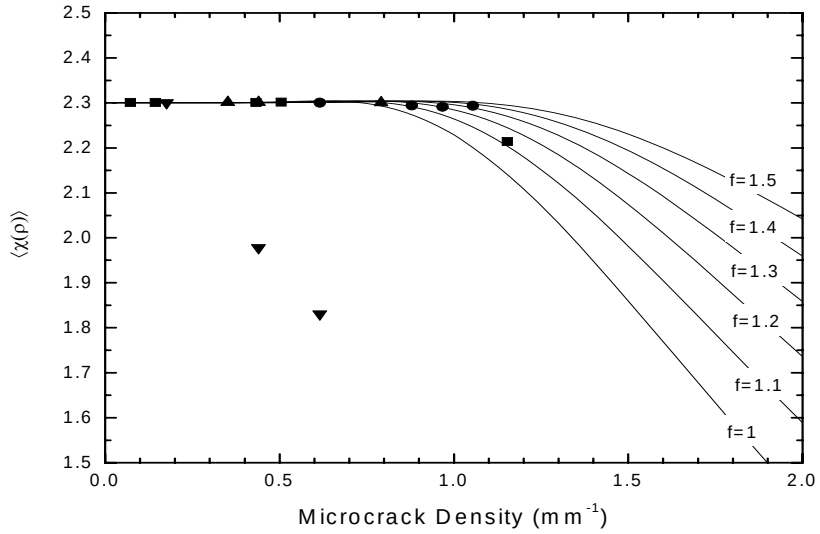


***Figure 4.13*** *The measured value of χ (ρ) and the predicted value of χ (ρ) for [0/90]s IM7/977-2 laminate.*

In using this method to determine *f*, it is expected that the experimental data for a particular sample would follow one of the theoretical curves, thus defining the value for *f*. As described earlier, IM7/977-2 did not reach the high crack density region (most data lie on a vertical line in the master curve in *Figure 4.12*). In this low crack density region, *χ(ρ)* is independent of *f*. Most of the experimental data points in *Figure 4.13* therefore lie along the horizontal portion of the curve. This method therefore fails for determination of the value of *f* from this data. An alternate method is followed to find *f* for each sample. The value for *f* is obtained by varying *f* in Equation (24) to get a best fit for the energy release rate equation (Equation 18). Again, the low crack density data points are not considered in the master-curve analysis. There were only six data points from IM7/977-2 which were in a high crack density region and those six data points are from 2 different samples 2-I-III-1 and 2-I-III-3. The calculated values of *f* using the best fit

method are 1.47 and 1.08 respectively for the above samples. The plot of master-curve for IM7/977 is shown in *Figure 4.14*. The values of *f* for the other samples can be taken as 1, since all the data are in the low crack density region where *f* has no effect.

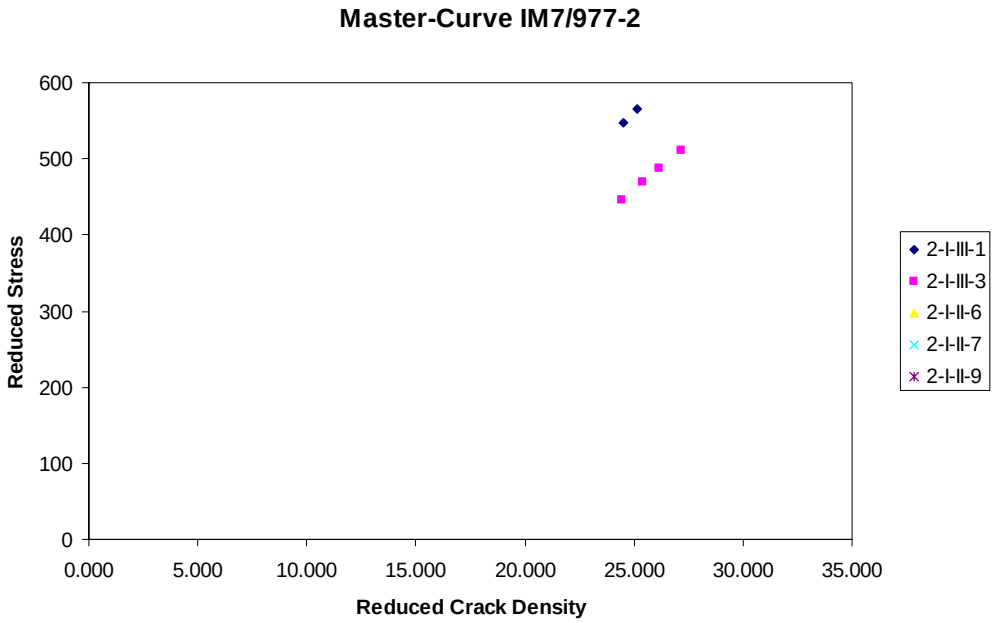


***Figure 4.14*** *Master-Curve analyses using best fit method*

Fitting these points as a single master curve produced unreasonable results. However, analyzing the master curve is plotted individually for these two samples and the average microcrack density obtained by the linear fit is 650 J/m$^2$ and the average $T_{eff}$ (intercept of the curve) is -125 °C. We can further analyze this data by plotting crack density as a function of applied stress. Theoretical curves can be obtained by back calculating the applied stress from equation (25) with a given value of Gm. *Figure 4.15* and *Figure 4.16* show the comparison of such plots with the average fracture toughness obtained (610 J/m$^2$) from finite fracture toughness calculations including the

low crack density data, and the average fracture toughness obtained from master-curve analysis (650 J/m$^2$) excluding the low crack density data.

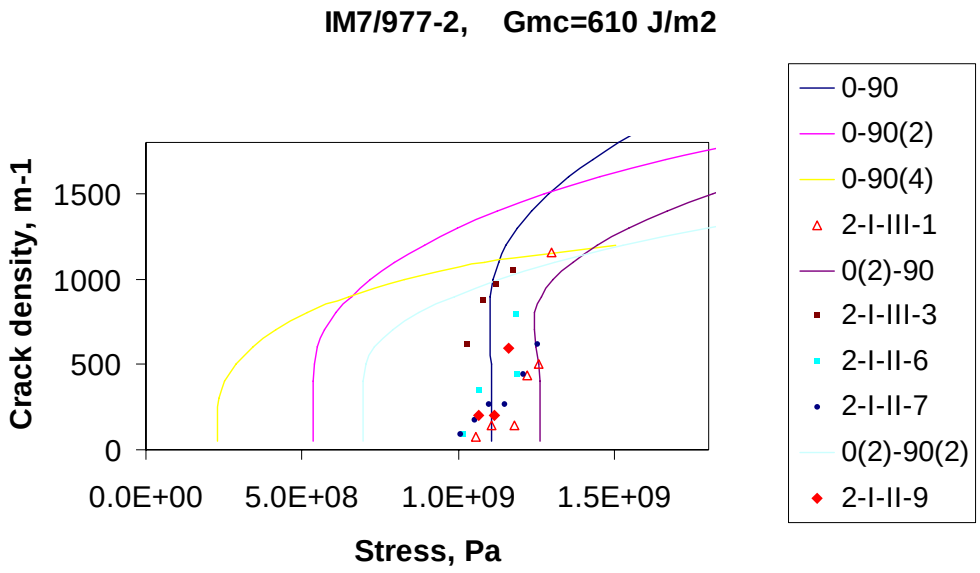


***Figure 4.15*** *The microcrack density as a function of applied load in IM7/977-2. The symbols are experimental data points and the smooth lines are using Gm=610J/m$^2$*

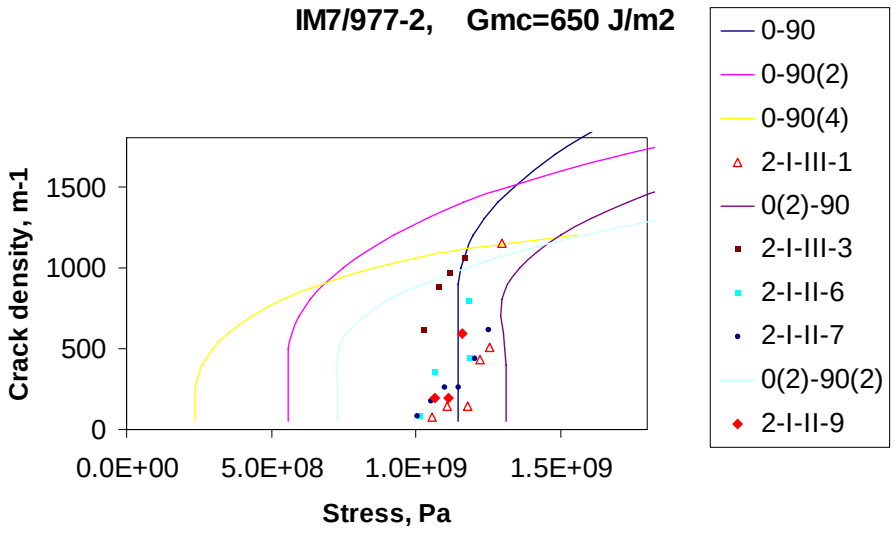


***Figure 4.16*** *The microcrack density as a function of applied load in IM7/977-2. The symbols are experimental data points and the smooth lines are using Gm=650J/m$^2$*

### *4.2.2 IM7/5555*

The material properties for IM7/5555 were not provided by the manufacturer. They have been calculated using the rule of mixtures [Ref 35]. The properties of the fiber ($E_f$ = 276GPa) and the matrix ($E_m$ = 2.9 GPa) were obtained from their manufacturers [Ref 36]. The volume fractions ($V_f$ = 0.57 and $V_m$ = 0.43) used for this material system are estimated from the previous material system IM7/977-2. The material properties obtained are listed in *Table 4.8* and the calculations are shown in the Appendix.

***Table 4.8*** *Input material properties for IM7/5555. *Please note that these are not the accurate material properties but are estimated based on the individual material properties of the fibers and matrix.*

| **Property** | **Value*** |
|---|---|
| $E_a$ ( Axial Modulus ply material ) | 158.57GPa |
| $E_t$ ( Transverse Modulus of ply material ) | 6.65GPa |
| $E_c$ (x- direction modulus of cross-ply laminate) | 82.6GPa |
| $G_a$ (Axial Shear modulus) | 5.47GPa |
| $G_t$ (Transverse Shear modulus) | 2.22GPa |
| $\alpha_a$ (Axial thermal expansion coefficient ) | -0.09 ppm/$^o$C |
| $\alpha_t$ (Transverse thermal expansion coefficient) | 28.8 ppm/$^o$C |
| $v_a$ ( Axial Poisson's Ratio) | 0.253 |
| $v_t$ ( Transverse Poisson's Ratio) | 0.456 |
| $T_{eff}$ ( Stress free temperature) | -125 $^o$C |

The values $\alpha_a$ and $\alpha_t$ were taken from [Ref 4] as they are common for most material systems. $T_{eff}$, the stress-free temperature, is basically the difference between the curing temperature (177$^o$C) and room temperature (24$^o$C). To account for the possibility of some relaxation at high temperatures $T_{eff}$ is taken to be -125$^o$C. The ply thickness is same for all the material systems and is 0.1375mm. The master plot for IM7/5555 without using *f* is shown in *Figure 4.17*.

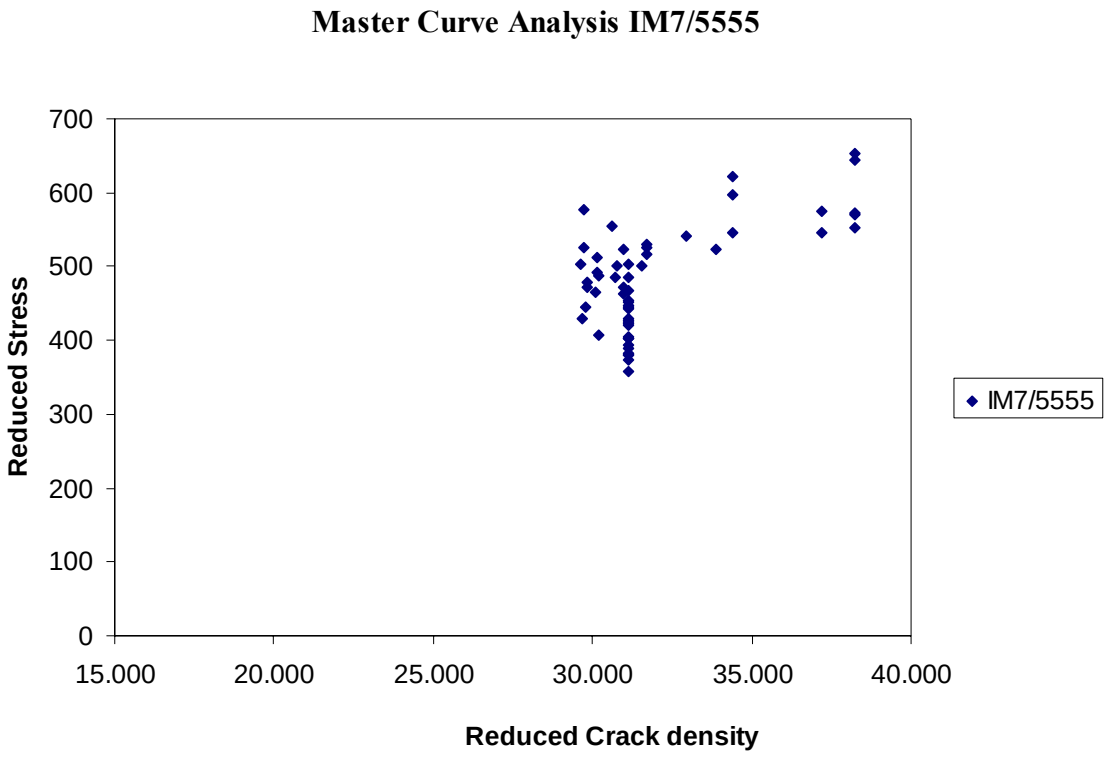


***Figure 4.17*** *Master curve analysis of a* $[0/90]_s$ *IM7/5555 laminate*

Again the alternate method is followed to find *f* for each sample by varying *f* in Equation (24) to get a best fit for the master plot and the fracture toughness is measured from the master plot obtained. Again, the low crack density data points are not considered in the master-curve analysis. The calculated values of *f* using the best fit method varied from 1.035 to 1.558 for the samples of the IM7/5555 material system. The plot of the master-curve for IM7/5555 is shown in *Figure 4.18*.

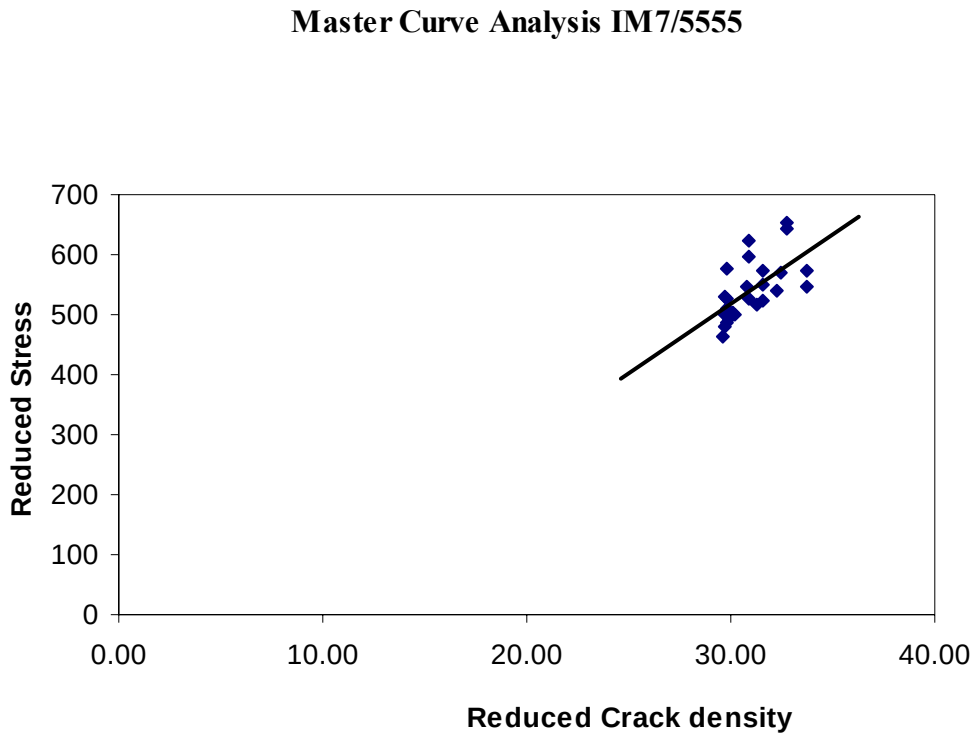


***Figure 4.18*** *Master-curve analysis for IM7/5555, the intercept (Teff) = -125 and (slope)$^2$ (Fracture Toughness, Gm,) = 467J/m$^2$*

The average microcrack density obtained by the linear fit of the above master plot is 467 J/m$^2$ and the average $T_{eff}$ (intercept of the curve) is -125 $^0$C.

### *4.2.3 IM7/5276-1*

The material properties for IM7/5276-1 were not provided by the manufacturer. They have been calculated using rule of mixtures [Ref 35]. The properties of the fiber ($E_f$ = 276GPa) and matrix ($E_m$ = 3.05 GPa) were obtained from a different manufacturer [Ref 36]. The volume fractions ($V_f$ = 0.57 and $V_m$ = 0.43) used for this material system are estimated from the previous material

system IM7/977-2. The material properties obtained are listed in *Table 4.9* and the calculations are shown in the Appendix.

***Table 4.9*** *Input material properties for IM7/5276-1. * Please note that these are not the accurate material properties but are estimated based on the individual material properties of the fibers and matrix*

| **Property** | **Value*** |
|---|---|
| $E_a$ ( Axial Modulus ply material ) | 158.63GPa |
| $E_t$ ( Transverse Modulus of ply material ) | 6.98GPa |
| $E_c$ (x- direction modulus of cross-ply laminate) | 82.6GPa |
| $G_a$ (Axial Shear modulus) | 5.47GPa |
| $G_t$ (Transverse Shear modulus) | 2.23GPa |
| $\alpha_a$ (Axial thermal expansion coefficient ) | -0.09 ppm/$^o$C |
| $\alpha_t$ (Transverse thermal expansion coefficient) | 28.8 ppm/$^o$C |
| $v_a$ ( Axial Poisson's Ratio) | 0.253 |
| $v_t$ ( Transverse Poisson's Ratio) | 0.456 |
| $T_{eff}$ ( Stress free temperature) | -125 $^o$C |

The values $\alpha_a$ and $\alpha_t$ were taken from [Ref 4] as they are common for most material systems. $T_{eff}$, the stress-free temperature, is basically the difference between the curing temperature (177$^o$C) and room temperature (24$^o$C). To account for the possibility of some relaxation at high temperatures $T_{eff}$ is taken to be -125$^o$C. The ply thickness is same for all the material systems and is 0.1375mm. The master plot for IM7/5276-1 without using *f* is shown in *Figure 4.19*.

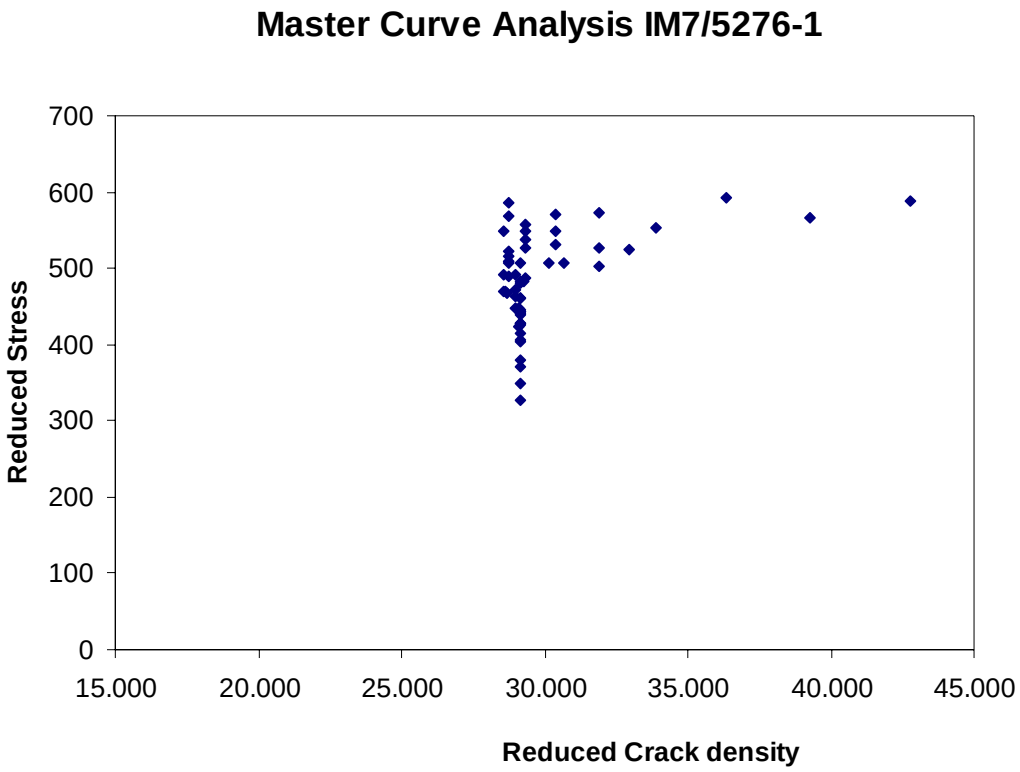


***Figure 4.19*** *Master curve analysis of $[0/90]_s$ IM7/5276-1 laminate*

Again the alternate method is followed to find *f* for each sample by varying *f* in Equation (24) to get a best fit for the master plot and the fracture toughness is measured from the master plot obtained. Again, the low crack density data points are not considered in the master-curve analysis. The calculated values of *f* using the best fit method varied from 1.02 to 1.45 for the samples of the IM7/5276-1 material system. The plot of master-curve for IM7/5555 is shown in *Figure 4.20*.

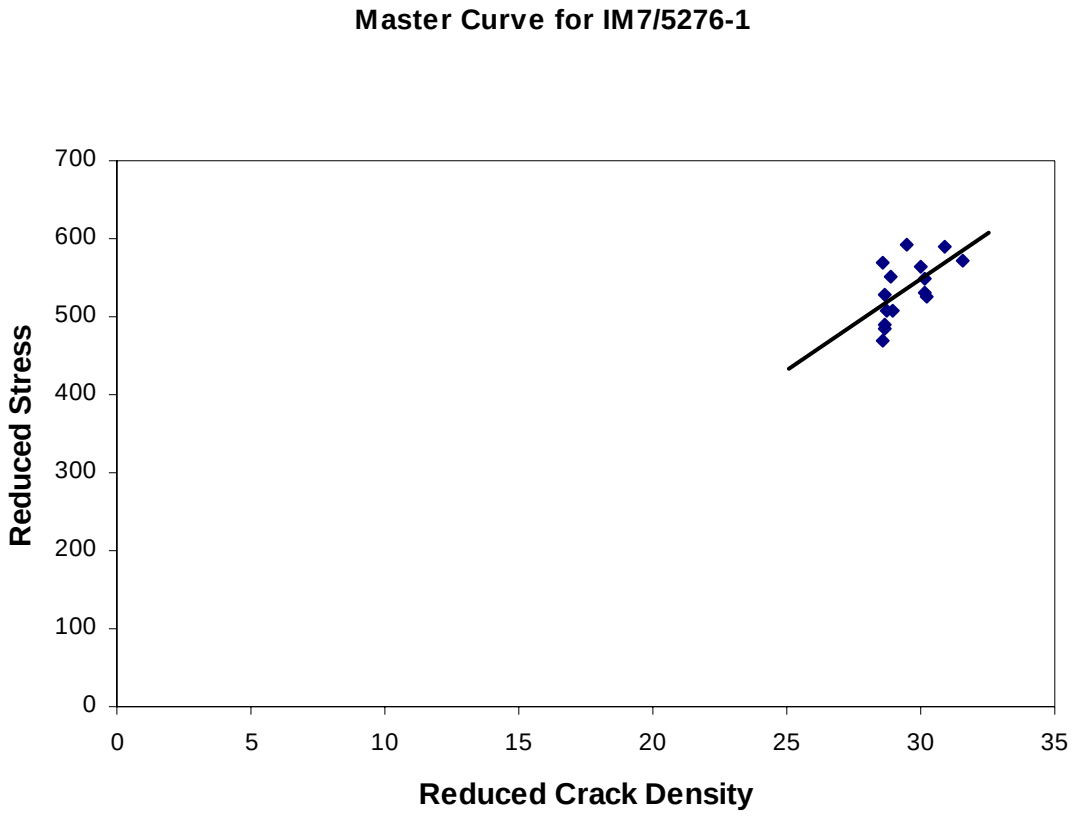


***Figure 4.20*** *Master-curve analysis for IM7/5276-1, the intercept (Teff) = -125 and (slope)$^2$ (Fracture Toughness, Gm,) = 504 J/m$^2$*

The average microcrack density obtained by the linear fit of the above master plot is 504 J/m$^2$ and the average $T_{eff}$ (intercept of the curve) is -125 $^0$C.

# 5. Conclusions and Recommendations

An important material property, microcracking fracture toughness, Gm, was calculated for all the three material systems IM7/977-2, IM7/5555 and IM/5276-1. It is observed that the three material systems with $[0/90]_s$ orientation are resistant to microcracking below 800 MPa stress under mode I loading. The onset of microcraking in the composite laminates IM7/977-2, IM7/5555 and IM/5276-1 occurs at 1050MPa, 850MPa and 950MPa respectively. IM7/5555 is the only system that displayed saturation in the crack density (~17 cracks per cm). From the plots of microcracking density versus applied stress it was observed that in the material system IM7/977-2 microcrack initiation starts at higher loads and the material system fails much faster (within 250 MPa of additional stress). The material systems IM7/5555 and IM/5276-1 showed microcracking initiation at lower loads and the microcracking density increases gradually with applied stress.

The microcracking fracture toughness for material systems IM7/977-2, IM7/5555 and IM/5276-1 were calculated to be around 610-650 $J/m^2$; 470 $J/m^2$ and 500 $J/m^2$ respectively. From these values it is also evident that material system IM7/977-2 is more resistant to crack initiation when compared to the other two and IM7/5555 being the weakest among all.

Increasing the optical span length to cover the gage length of the sample would lend more information regarding the damage behavior. Inspecting the samples at smaller load increments could potentially yield higher crack density information; this could be particularly useful in

examining the *f* parameter for the IM7-977-2 samples. Investigating other ply lay-ups for the IM7/977-2 material would give a better understanding of the microcracking behavior.

As the manufacturer did not provide the material properties, another challenging task would be measuring the material properties for material systems IM7/5555 and IM7/5276-1, including the shear modulus. The Young's modulus can be calculated by performing regular tensile tests on both [0/90]s and [90/0]s laminates and the shear modulus can be measured using strain gauges while testing the samples.

# References


1. Dixon. S.C, Tenny. D.R, Rummler. D.R, Weiting. A and Bader. M, *"Structures and Material Technology Issues for Reusable Launch Vehicles,"* NASA TM- 87626, October 1985.

2. Melody A. Verges, Paul Schilling, Paul D. Herrington and Arun K. Tatiparthi, *"Investigation of Microcrack Growth in [0/90]$_S$ Composite Laminates"*, ASME Pressure Vessels Piping Div Publ, (2003) 171-175.

3. *"Final Report of the X-33 Failure Investigation Team,"* X-33: Reusable Launch Vehicle – Space Transportation [online database], URL: http://x33.msfc.nasa.gov [cited 24 Jan. 2001]

4. J. A. Nairn, *"Matrix Microcracking in Composites"*. Polymer Matrix composites (edited by R. Talreja and J.-A. E. Manson), Volume-2 of comprehensive Composite Materials, Elsevier Science, pp.403-432 (2000).

5. S. Liu and J.A. Nairn, *"The Formation and Propagation of Matrix Microcracking in Cross-Ply Laminates during Static Loading",* J. Reinf. Plast. and Comp. 11 (1992) 158-178.

6. Simon Frost, Richard Lee, Mark Stone, *"Assessment & Criticality of Defects & Damage in Materials Systems"* Task 1 Review, AEA Technology, MMS13 IAG, November 2002.

7. Michael Gower, Graham Sims*, "Assessment & Criticality of Defects & Damage in Materials Systems"* Task 1 Review, National Physical Laboratory, MMS13 IAG, November 2002.

8. R. Joffe*, "Damage Accumulation and Stiffness Degradation in Composite Laminates",* Doctoral Thesis.

9. Kunigal N. Shiva Kumar, *"Course MEEN860 – Fracture Mechanics"*, North Carolina A&T State University.

10. John A. Nairn, Shoufeng. Hu and Jong Song Bark, *"Master plot analysis of Microcracking in Graphite/epoxy and Graphite/PEEK laminates".* Third NASA Advanced Composite Technology Conference proceedings of a workshop, June8-11,1992, pp.557

11. M. G. Bader, J. E. Bailey, P. T. Curtis, and A. Parvizi, *"The Mechanisms of Initiation and Development of Damage in Multi-Axial Fiber-Reinforced Plastics Laminates"*. Proceedings of 3rd Int'l Conf. on Mechanical Behavior of Materials 3 (1979), pp.227-239.

12. J. E. Bailey, P. T. Curtis and A. Parvizi, *"On the Transverse Cracking and Longitudinal Splitting Behavior of Glass and Carbon Fiber Epoxy Cross-Ply Laminates and the Effect of Poisson and Thermally Generated Strains"*. Proc. R. Soc. Lond. A 366 (1979), pp.599-623.

13. Groves, S. E, Harris, C. E, Highsmith, A. L, and Norvell, R. G, *"An Experimental and Analytical treatment of Matrix Cracking in Cross-Ply Laminates"*. Experimental Mechanics, vol. March, 1987, pp. 73-79

14. K. W. Garrett and J. E. Bailey, *"Multiple Transverse Fracture in 90± Cross-Ply Laminates of a Glass Fiber-Reinforced Polyester"*. Journal of Material Science, Volume-12 (1977), pp.157-168.

15. K. W. Garrett and J. E. Bailey, *"The Effect of Resin Failure Strain on the Tensile Properties of Glass Fiber-Reinforced Cross-Ply Laminates"*. Journal of Material Science, Volume-12 (1977), pp.2189-2194.

16. Parvizi, K. W. Garrett, and J. E. Bailey, *"Constrained Cracking in Glass Fiber-Reinforced Epoxy Cross-Ply Laminates"*. Journal of Material Science, Volume-13 (1978), pp.195-201.

17. P. A. Smith, L. Boniface, and N. F. C. Glass, *"A Comparison of Transverse Cracking Phenomena in (0/90)s and (90/0)s CFRP Laminates"*. Applied Composite Materials. Volume-5 (1998), pp.11-23.

18. L. Highsmith and K. L. Reifsnider, *"Stiffness-Reduction Mechanisms in Composite Laminates"*. ASTM STP 775 (1982), pp.103-117. 77

19. J. A. Nairn, *"Microcracking, Microcrack-Induced Delamination, and Longitudinal Splitting of Advanced Composite Structures"*. NASA CR 4472 (1992).

20. W. W. Stinchcomb, K. L. Reifsnider, P. Yeung, and J. Masters, *"Effect of Ply Constraint on Fatigue Damage Development in Composite Material Laminates"*. ASTM STP 723 (1981), pp.64-84.

21. J. A. Nairn, S. Hu, S. Liu, and J. S. Bark, *"The Initiation, Propagation, and Effect of Matrix Microcracks in Cross-Ply and Related Laminates"*. Proc. of the 1st NASA Advanced Composite Tech. Conf. Seattle, WA, Oct. 29 to Nov. 1, 1990 (1990).

22. L. Berglund and J. Varna, *"Transverse Cracking and Local Delamination in [04=90n]s and [90n=04]s Carbon Fiber/Toughened Epoxy Laminates"*. Journal of Reinforced Plastic & Composites. Volume-11 (1992), pp.643-660.

23. J. A. Nairn and S. Hu, *"The Formation and Effect of Outer-Ply Microcracks in Cross-Ply Laminates: A Variational Approach"*. Engineering Fracture Mechanics, Volume-41 (1992), pp.203-221.

24. D. L. Flaggs and M. H. Kural, *"Experimental Determination of the In Situ Transverse Lamina Strength in Graphite/Epoxy Laminates"*. Journal of Material Science, Volume-16 (1982), pp.103-115.

25. John A. Nairn, *"Finite Fracture Mechanics of Matrix Microcracking in composites"*. Polymer Matrix composites

26. J. A. Nairn, S. Hu, and J. S. Bark, "*Journal of Material Science"*. 28, 1993, 5099-5111.

27. Z. Hashin "*Journal of Mechanics & Physics of Solids"* 44, 1996, 1129-1145.

28. J. A. Nairn and S. Hu in *Damage Mechanics of Composite Materials*, eds., Ramesh Talreja, Elsevier Science, The Netherlands, 1994, 187-243.

29. J. A. Nairn in *Polymer Matrix Composites*, eds., R. Talreja and J.-Å. E. Manson, Elsevier Science, The Netherlands, 2000, 403-432.

30. J. A. Nairn, *5th Int'l Conf. on Def. and Fracture of Composites*, London, UK, March - 1999, pp.18-19.

31. Nairn, J. A, "Journal of Composite Materials", 23, 1989, pp.1106

32. Hashin, Z *"Mechanics of Materials"*, 1985, 4:121.

33. Hashin, Z *"Engineering Fracture Mechanics"*, 1986, 25:771.

34. John, A. Nairn, Shoufeng Hu, Jong, S. Bark, *"A critical evaluation of theories for predicting microcracking in composite laminate"*. Journal of material science, Vol.28, September 1993, pp.5099-5111.

35. David Roylance, *"Introduction to Composite materials"* Department of Materials Science and Engineering, Massachusetts Institute of Technology, March 24, 2000

36. CYTEC, *"Engineered Materials"*, http://www.cytec.com, www.hexcel.com and www.tohotenaxamerica.com

37. Babruvahan Hottengada, *"Investigation of Microcracking and damage propagation in cross-ply Composite Laminates"*, Master's Thesis, University of New Orleans.

# Appendix

## *Material properties for IM7/5555*

From Ref [36] the properties of IM7 and 5555 are given as

$E_f$ =276 GPa and $E_m$ = 3.52 GPa

The volume fractions are calculated from the properties of IM7/977-2 (provided by the manufacturer.

$V_f$ = fiber volume fraction = 0.57

$V_m$ = matrix volume fraction = 0.43

According to the rule of mixtures [Ref 35], axial modulus of the laminate is given by

$$E_a = V_f E_f + V_m E_m$$

$E_a = 0.57(276) + 0.43(3.52)$

$E_a$ = 158.567 GPa

The transverse modulus of the laminate is given by

$$\frac{1}{E_T} = \frac{V_f}{E_f} + \frac{V_m}{E_m}$$

$$\frac{1}{E_T} = \frac{0.57}{276} + \frac{0.43}{3.52}$$

$$E_T = 6.652 MPa$$

There was not enough data to calculate the shear modulus of the laminate. I researched the technical papers by Nairn and from Nairn [Ref 5], I was able to find a reasonable relation between tensile modulus and shear modulus. The values I used here are the transverse shear

modulus of laminate is one third the transverse tensile modulus and the axial shear modulus of the laminate is one twenty ninths the axial tensile modulus.

Thus the calculated shear moduli for IM7/5555 are

$G_a = E_a/29 = 158.567/29 = 5.468$ GPa

$G_T = E_T/3 = 6.651542/3 = 2.2171$ GPa

### *Material properties for IM7/5276-1*

From Ref [36], the tensile modulus of G40-800 fiber is $E_f = 290$ GPa (G40-800)

$V_f$ = fiber volume fraction = 0.53

$V_m$ = matrix volume fraction = 0.47

From Ref [36], The tensile modulus of the laminate G40-800/5276-1 is

Ea = 22.5 Msi = 155132 MPa

According to the rule of mixtures [Ref 35], the axial tensile modulus of the laminate is given by

$$E_a = V_f E_f + V_m E_m$$

155.132= 0.53 (290) + 0.47 ($E_m$)

155.132 = 153.7 +0.4 $E_m$

1.432 = 0.4 $E_m$

$E_m$ = 3.0468 GPa

From Ref [36] the properties of IM7 are given as $E_f$ =276 GPa

The volume fractions are calculated from the properties of IM7/977-2 (provided by the manufacturer.

$V_f$ = fiber volume fraction = 0.57

$V_m$ = matrix volume fraction = 0.43

Again from the rule of mixtures [Ref 35], axial modulus of the laminate is given by

$$E_a = V_f E_f + V_m E_m$$

$E_a = 0.57(276) + 0.43(3.0468)$

$E_a = 158.6302$ GPa

The transverse modulus of the laminate is given by

$$\frac{1}{E_T} = \frac{V_f}{E_f} + \frac{V_m}{E_m}$$

$$\frac{1}{E_T} = \frac{0.57}{276} + \frac{0.43}{3.0468}$$

$$E_T = 6.9838 MPa$$

There was not enough data to calculate the shear modulus of the laminate. I researched the technical papers by Nairn and from Nairn [Ref 5], I was able to find a reasonable relation between tensile modulus and shear modulus. The values I used here are the transverse shear modulus of laminate is one third the transverse tensile modulus and the axial shear modulus of the laminate is one twenty ninths the axial tensile modulus.

Thus the calculated shear moduli for IM7/5276 are

$G_a = E_a/29 = 158.5302/29 = 5.470$ GPa

$G_T = E_T/3 = 6.9838/3 = 2.32795$ GPa

# Vita

Krishna Kumar Kasturi was born on November 22, 1978 to Sattiah and Sujatha Kasturi in Karimnagar, India. He graduated from Vignan Co-operative Junior College in 1996 and obtained his Bachelor's of engineering degree in Mechanical Engineering from Osmania University, India in 2001. He joined the graduate program in Mechanical Engineering at University of New Orleans in 2002. He accepted a position as graduate teaching assistance with department of mechanical engineering in Fall2002. During his tenure as a teaching assistant he got a chance to work with Dr. Paul J. Schilling and accepted a position as graduate research assistant with Dr. Paul J. Schilling in Fall2003. Since then he has worked on different projects under the guidance of Dr. Paul J. Schilling. In August of 2006, he earned his Masters of Science degree in Mechanical Engineering with a thesis entitled "Master curve analysis for graphite-epoxy composite laminates using finite fracture mechanics."